



HAL
open science

Determinants of rear-of-wheel and tire-road wear particle emissions by light-duty vehicles using on-road and test track experiments

A. Beji, K. Deboudt, S. Khardi, B. Muresan, L. Lumière

► **To cite this version:**

A. Beji, K. Deboudt, S. Khardi, B. Muresan, L. Lumière. Determinants of rear-of-wheel and tire-road wear particle emissions by light-duty vehicles using on-road and test track experiments. Atmospheric Pollution Research, 2021, 12 (3), pp.278-291. 10.1016/j.apr.2020.12.014 . hal-04290952

HAL Id: hal-04290952

<https://ulco.hal.science/hal-04290952>

Submitted on 22 Nov 2023

HAL is a multi-disciplinary open access archive for the deposit and dissemination of scientific research documents, whether they are published or not. The documents may come from teaching and research institutions in France or abroad, or from public or private research centers.

L'archive ouverte pluridisciplinaire **HAL**, est destinée au dépôt et à la diffusion de documents scientifiques de niveau recherche, publiés ou non, émanant des établissements d'enseignement et de recherche français ou étrangers, des laboratoires publics ou privés.

1 Determinants of rear-of-wheel and tire-road wear particle emissions
2 by light-duty vehicles using on-road and test track experiments
3

4 A. Beji¹, K. Deboudt², S. Khardi¹, B. Muresan^{1*}, L. Lumière¹
5

6 ¹ Environment-Planning, Safety and Eco-design (EASE-AME) Laboratory, Gustave Eiffel
7 University, 77454 Marne-la-Vallée, France (EU).

8 ² Laboratory of Physical Chemistry of the Atmosphere (LPCA), Littoral Côte d'Opale
9 (ULCO) University, 59140 Dunkerque, France (EU).

10

11

12

13

14

15

16

17

18

19

20

21

22 *: Corresponding author

23 Email: bogdan.muresan-paslaru@univ-eiffel.fr

24 Mailing address: Allée des Ponts et Chaussées CS 5004 44344 Bouguenais, France (EU)

25 Phone: +33(0)2 4084 5635 / Fax: +33(0)2 4084 5999

26 **Abstract**

27 The purpose of this study is to identify the parameters governing particle emissions at the rear
28 of the front wheel of an instrumented light-duty vehicle. The information obtained from the
29 road is complemented by data acquired on a test track. By comparing the signals recorded at
30 various locations around the vehicle, a distinction can be drawn between rear of the wheel
31 particles (RoWP) and particles resulting from tire and road wear (TRWP). Both types of
32 emissions are highly dependent on driving speed. TRWP mainly fall in the size ranges of <
33 0.03 μm and 0.05-0.30 μm by their number, and 0.1 - 0.6 μm and 1.0 - 15 μm by mass when
34 using a mean density of 2.0 g/cm^3 . Within these ranges, TRWP account on average for 40%
35 and 25% of RoWP emissions, respectively. We also evaluate herein the influence of: i)
36 pavement contamination by particulate matter, ii) road geometry, iii) driving area, and iv)
37 structural elements affecting road traffic. Test track experiments finally provide information
38 on the significance of accelerations, decelerations, pavement texture and age. This knowledge
39 compilation may be implemented in future non-exhaust particulate emissions standards;
40 moreover, it establishes a basis for realistically assessing emission dynamics and identifying
41 affected areas.

42 Keywords: Particles, tire and road wear, mobile measurements, emission determinants, high-
43 emission situations.

44

45 **Highlights:**

46 Rear of wheel particulate emissions were assessed on the road and on a test track.

47 Both rear of wheel and tire-road wear particle emissions increase with speed.

48 Particulate deposits on tires and roads further increase emissions.

49 Urban cores would not be the most conducive to these emissions, but rather suburban areas.

50 Test track data provide a better understanding of the role of pavement type, texture and age.

51

52 **1. Introduction**

53 Since exhaust particulate emissions are subject to increasingly stringent standards, the share
54 of non-exhaust particulate (NEP) emissions is bound to increase. In nearly thirty years,
55 European standard thresholds for exhaust particulate emissions have been reduced by a factor
56 of over 30 (from 140 mg/km to below 4.5 mg/km between the Euro 1 and Euro 6d standards)
57 (EEA, 2016). This reduction has been implemented despite strong differences between
58 measurements carried out on the road and on chassis dynamometers (ICCT, 2017; ECA,
59 2019). Over the past few decades, attention has been shifted to NEP emissions, especially
60 particles emitted by the braking system or the tire-road interface. The increasing complexity
61 of materials used in brake pads and tires, coupled with the limited amount of updated
62 information provided by manufacturers, would suggest that a vast field of study will emerge
63 in the coming years (Blau, 2001; Camatini *et al.*, 2001; Lindenmuth, 2006). In addition, the
64 toxicity of chemical compounds used in materials' manufacturing (heavy metals, persistent
65 organic compounds, flame retardants, endocrine disruptors, nanopowders, etc.) underscores
66 the potential of NEP to exert adverse effects on the health of ecosystems adjacent to roads, as
67 well as on the human populations inhabiting these ecosystems (Kreider *et al.*, 2010; Amato,
68 2018; Charron *et al.*, 2019).

69 It is widely accepted that the atmospheric loading of NEP can be comparable to that of
70 exhaust particles (Querol *et al.*, 2001; Lenschow *et al.*, 2001) and will ultimately dominate
71 due to the transition toward hybrid and electric vehicles. In urban areas, NEP emissions are
72 estimated to account for a few tens of percent up to > 70% of PM₁₀ (i.e. a class of particles
73 with a mean diameter of 10 µm) (Lenschow *et al.*, 2001; Querol *et al.*, 2004; Thorpe *et al.*,
74 2007; Harrison *et al.*, 2012). In a city street environment, tire fragments produced by wear can
75 alone constitute between 1 and 10 µg/m³ of air or a few percent of PM₁₀ (nearly 460,000 tons
76 of rubber were dispersed along European roads in 2006: Wik and Dave, 2009). NEP emission
77 factors identified in databases (Copert 4, EMEP and PIARC) and the literature (Abu-Allaban
78 *et al.*, 2003; Ketznel *et al.*, 2007; Bukowiecki *et al.*, 2010) range from less than 5
79 mg/km/vehicle to as high as 50 mg/km/vehicle for passenger cars and from 100
80 mg/km/vehicle to over 1,000 mg/km/vehicle for heavy trucks. The relative contributions of
81 resuspension and wear (tires, brakes, road surface) to NEP emissions lie on the order of 50/50
82 for passenger cars and 75/25 for heavy-duty vehicles. However, these ratios should only be
83 considered as a guide since they depend on many variables, including vehicle dynamics, tire
84 and road surface properties, and weather conditions.

85

86 Studies devoted to characterizing tire wear particles (TWP) have been mostly based on
87 roadside and laboratory measurements using tire simulators (such as inner and outer drum test
88 benches); moreover, they more rarely comprise experiments carried out on the road (Kwak *et al.*,
89 *et al.*, 2013, 2014; Pirjola *et al.*, 2010). Simulations demonstrate that the particles collected at
90 the rear of instrumented wheels (RoWP) can be smaller than expected (Thorpe and Harrison,
91 2008). Depending on the simulated driving conditions, RoWP would fall in the ultrafine
92 (peaking at 20-30 nm), fine (approx. 50% by mass of emitted PM₁₀) and coarse size classes
93 (Grigoratos *et al.*, 2018). The RoWP generated by means of drum test benches originate
94 mainly from tire wear, while bearing in mind that for any given vehicle, only 15% of the
95 RoWP > 0.3 µm collected on the road actually come from its own tires (Kreider *et al.*, 2010).
96 RoWP emissions measured in the laboratory and on the road may however differ, as a result
97 of: the impossibility of completely reproducing the stresses that develop at the tire-road
98 interface; the resuspension induced by the vehicle body or nearby traffic; weathering and
99 variations in asphalt concrete roughness, including contamination by dust from the nearby
100 environment and multiple road traffic emissions.

101 In fact, measurements conducted on the road lend insight into the complexity of the emission
102 mechanisms of both RoWP and abraded particles (i.e. from tires and the road surface:
103 TRWP). This complexity can in part be resolved by coupling on-road measurements with data
104 obtained under semi-controlled conditions, which are reflective of actual driving conditions.
105 This study investigates the influence of driving conditions and road texture on the emission
106 dynamics and size distribution of RoWP and TRWP. The data acquired seek to answer the
107 following question: “What are the determinants for RoWP emissions on the road, and to what
108 extent do these determinants also affect the dynamics of TRWP emissions?” Our search for an
109 answer led to employing a two-step strategy involving a simultaneous on-road assessment of
110 vehicle parameters and particulate emissions followed by a test track investigation of the
111 relevant parameters previously identified. The results obtained have made it possible to
112 propose mechanisms that explain the dynamics of RoWP and TRWP emissions on the road,
113 as well as strategies to limit emissions depending on the vehicle dynamics, road surface
114 properties or the type of driving area.

115

116 **2. Materials and methods**

117 **2.1 Vehicle instrumentation**

118 This research was carried out by using specially equipped vehicles operated by the Gustave
119 Eiffel University. In all, 8 vehicles were instrumented, composed of 7 passenger cars and a
120 van. The results proposed herein stem from measurement series representative of emission
121 trends under actual traffic conditions recorded by a fully-instrumented vehicle, i.e. a Renault
122 Clio 3, 1.6i 16V, 111 hp (one of the most common models found in France). This vehicle is
123 gasoline-powered, subject to the Euro 4 emission standard and fitted with commercial
124 summer tires (MichelinTM Energy Saver, 185/60 R 15 88H), which feature asymmetrical
125 structures with three straight grooves running around the center of the rubber tread. The tire
126 surface is mostly amorphous, with Si fiber and Fe-enriched inclusions. The vehicle enables
127 accessing several key parameters related to engine operations and vehicle dynamics. These
128 parameters include: engine speed and acceleration, fuel consumption, wheel and ground
129 speeds, brake pressure, and steering angle. All parameters were monitored at a frequency of
130 10 Hz and continuously recorded by means of on-board computers.

131 In addition to the vehicle dynamics parameters, particle size distributions were recorded in
132 real-time using four devices: two Electrical Low Pressure Impactors (ELPI DekatiTM), and
133 two Optical Particle Counters (OPC GrimmTM EDM 1.108). The ELPI devices measured the
134 number size distribution of particles with an aerodynamic diameter lying between 0.007 and
135 10 μm , at a time step of 1 s. This device operates at a flow rate of 10 L/min, with 12 size
136 channels. The OPCs were introduced in order to probe, on an ancillary basis, the fine and
137 coarse mode particles. The method employed in an attempt to splice ELPI and OPC signals is
138 provided in Appendix 1. These devices output real-time measurements of particles with an
139 optical diameter lying between 0.35 and 22.5 μm ; they feature 15 size channels, a flow rate of
140 1.2 L/min and a time step of 6 s. All apparatuses used are calibrated by their manufacturers,
141 with calibrations being verified on a daily basis against similar devices operated by partners
142 (ensuring a signal discrepancy less than 20%). According to the manufacturers, the analytical
143 uncertainties on ELPI and OPC measurements are 5% and 3% respectively. However, these
144 percentages are only indicative as laboratory controls show that they are in fact closer to 7%
145 and 15%, in this order. Taking into account the sampling and particle transfer biases, the
146 overall accuracy of the measurements will be slightly higher than 80%. The mass size
147 distributions were assessed from the number size distribution in considering the particles as
148 spheres. Furthermore, it is worth noting that despite the differences in absolute RoWP
149 densities depending on their sources (pavement and tire wear, resuspension of recent and aged

150 dust from total vehicular emissions and the surrounding environment, salting, etc.), a
151 reference density of 2.0 g/cm^3 was used in the calculations. This value is reflective of a
152 compromise between the densities of the asphalt concrete, particulate contaminants deposited
153 on the pavement and TRWPs obtained in the laboratory (i.e. $1.5\text{-}2.7 \text{ g/cm}^3$; Klöckner *et al.*,
154 2019).

155 A trailer containing the scientific instrumentation, along with two power generators, was
156 hitched to the test vehicle. The trailer and analytical equipment made up nearly 30% of the
157 weight of the vehicle with three passengers on board. It resulted in a median fuel consumption
158 surplus of 25% (from 5.5 l/100 km to 6.8 l/100 km), which translated into a median increase
159 in longitudinal forces and torques at the tire-road interface of less than 10% (respectively
160 from 205 N to 220 N and 30 Nm to 35 Nm). This increase was much smaller than that
161 observed in most acceleration or braking situations, i.e. the longitudinal forces and torques
162 then exceed 500 N and 200 Nm , respectively.

163 We instrumented the front wheels because they are the drive wheels: that is, where the
164 stresses at the tire-road interface are the highest. They are also the wheels for which forces
165 and torques are recorded by the vehicle's on-board computer. In fact, if the measurements had
166 been taken at the rear wheels, it would have been more difficult to distinguish local TRWP
167 emissions. They would have been mixed with emissions generated at the front wheels or road
168 dust resuspended by turbulence under the vehicle floor (Appendix 2). Consequently, the air
169 intakes for particle collection were placed at the rear of the front tire (driver's side) and in the
170 backspace of the wheel near the braking system (Fig. 1). The former collection point pertains
171 to RoWP, whereas the latter is focused on particles emanating from resuspension and the
172 braking system during strong decelerations. The proportion of TRWP was approximated by
173 subtracting the normalized concentrations measured in the backspace of the wheel from those
174 of RoWP (see Section 3.2). The air intake for RoWP was set 15 cm behind the tire and 7 cm
175 above ground. It was oriented so as to form a 15-degree angle with the vertical, thus
176 constituting an intermediate position intended to capture particles originating from both the
177 tire-road interface and the resuspension induced by tire action (Thivolle-Cazat and Gilliéron,
178 2006; Rajaratnam and Walker, 2019). Under such conditions, the airflow velocity was nearly
179 80% less than the vehicle speed (Kwak *et al.*, 2013) and barely influenced by the ambient
180 wind direction (Etyemezian *et al.*, 2003). According to preliminary numerical simulations
181 carried out using the Ansys Fluent code line, the angle between the sample intake and these

182 streamlines stemming from the tire-road interface varied from 40° at 30 km/h to 60° at 110
183 km/h.

184 2.2 Calculation of emissions and correction factors

185 Preliminary measurements and fluid dynamics simulations on the positioning and orientation
186 of the air intake served to assess particulate emissions toward the rear of the wheel (E) as well
187 as the aspiration efficiency of the instruments (η). The emission E (expressed in particles or
188 mg per sec or, upon division by driving speed, in particles or mg per km) was calculated as
189 follows:

$$190 \quad E = \frac{\mu \overline{U_0} \overline{C} A}{\eta} \quad (\text{Equation 1})$$

191 where “ μ ” is a correction factor for the change in streamline orientation (Fig. 1) based on
192 driving speed and steering angle (from < 0.05 to 1.2, with an average of 0.85 for on-road
193 measurements). “ $\overline{U_0}$ ” is the mean free flow velocity at the rear of the wheel (a linear
194 function of driving speed, in m/s) and “ \overline{C} ” the related mean concentration of particles (in
195 particles/m³ or mg/m³). Based on the results of preliminary numerical simulations, this
196 calculation assumed a parabolic shape of both airflow velocity and concentration profiles in
197 the horizontal plane. Their optima were the ones measured at the sampling point. “A” is the
198 area of a surface beneath the vehicle containing the sampling point; it averages 0.03 m² and is
199 determined by the intersection of streamlines from the tire-road interface and a plane
200 perpendicular to the driving direction. Like with the positioning and orientation of the air
201 intake, the change in A with increasing driving speed and steering angle (i.e. decrease and
202 increase, respectively) was determined beforehand and expressed by correction factor μ . The
203 values of η were estimated using an empirical approach developed by Belyaev and Levin
204 (1974) and then applied in Kwak *et al.* (2013), i.e.:

$$205 \quad \eta = 1 + \left[\left(\frac{U_0}{U} \right) \cos \theta - 1 \right] \left\{ 1 - \frac{1}{1 + (2 + 0.62 \frac{U_0}{U}) \text{Stk}} \right\} \quad (\text{Equation 2})$$

206 where U is the intake velocity and Stk the Stokes number. The total uncertainty (including
207 analytical and procedural steps) on emissions was estimated according to the error
208 propagation technique and lies between 10% and 60% (typically 25%). The influence of the
209 efficiencies of aspiration, tubing and the isokinetic probe will be detailed further below. The

210 calculated efficiencies were all close to 100% for particles smaller than 10 μm , i.e. for the
211 vast majority of relevant particles by number. The values were not as high for coarse particles
212 measured by OPC devices at speeds exceeding 70 km/h, thus leading to semi-quantitative
213 estimations in the 10-22.5 μm range ($0.7 < \eta < 1.7$). However, since particles larger than 10
214 μm account for less than 1% of accessible particles, the number-weighted emissions were not
215 corrected for this deviation.

216 The influence of tubing on measured concentrations was evaluated prior to sampling. The
217 tubing used to convey particles to the ELPI devices was 5-m long antistatic hoses with an
218 inner diameter of 8 mm. 3-m long antistatic hoses with a 4-mm inner diameter were used to
219 transport particles to the OPC device. Data show that the particle loss was insignificant (i.e.
220 less than 2%/m) and homogeneously distributed between fine and coarse particles: between <
221 1% and 3% variation in the ratio between fine (< 1 μm) and micrometric (> 1 μm) particle
222 number concentrations. Consequently, emissions were not corrected for this loss. It should be
223 noted that throughout the manuscript, statistical analyzes focused on correlation coefficients,
224 p-values and comparison of means using either Bonferroni or Holm-Šídák parametric tests (α
225 =0.05). These tests were performed after examining the independence, normality and
226 homoscedasticity of the data with XLSTAT and/or SIGMA PLOT applications. When
227 normality and homoscedasticity criteria were not met, analyzes were performed using
228 medians with the Kruskal-Wallis non-parametric test on ranks. The proposed results are
229 generally statistically significant at a 95% level.

230 Lastly, the influence of an isokinetic nozzle at the sample intake was examined by driving the
231 vehicle over the same roads in the presence or absence of nozzles (from TRC Tecora).
232 Concentrations were typically, but not systematically, lower in the absence of an isokinetic
233 nozzle. The change in the number-weighted concentration was nevertheless limited (ranging
234 from 3% to 9%) and increased with vehicle speed. The variation in the fine-to-micrometric
235 concentration ratio was lowest at 50 km/h, i.e. less than 3%, and did not exceed 15% (5% on
236 average) at speeds over 30 km/h. This finding likely reflects the decreased airflow velocity
237 observed at the rear of the tire and therefore the limited change in aspiration efficiency. The
238 variation in the fine-to-micrometric concentration ratio was greater at speeds below 30 km/h,
239 as illustrated by a decrease of approx. 15-40%, which can be attributed to the lower emission
240 rates of the instrumented vehicle and the significant influence of ambient road traffic.

241 **2.3 The reference test track**

242 A 2.3-km long test track with a maximum speed of 140 km/h was deployed in order to
243 evaluate RoWP and TRWP emission dynamics in a semi-controlled environment (Fig. S1).
244 This test track was equipped with 15 pavements composed of distinct wearing courses
245 representative of French and European roads or more specific road surfaces. This set-up made
246 it possible to test different qualities of tire-road contact, ranging from highly gritty textures to
247 the absence of gravel and therefore of macrotextures. Test track gravel originated from local
248 quarries: Le Cellier, Vrignaie, and Les Pontreaux. The coarsest gravel fraction (6-10 mm) was
249 rhyolite, while the 0-2 mm, 0-4 mm, 2-6 mm and, on rare occasion, the 4-10 mm fractions
250 were gneiss. As a mix design example, the proportions of the various fractions used to
251 construct the conventional test track pavement were: 0-4 mm (45%), and 4-10 mm (55%).
252 The relative percentage of bitumen 60/70 was 6.2% by mass.

253 The road surface texture can be divided into three major categories: microtexture,
254 macrotexture and megatexture (PIARC, 1995). Megatexture reflects the broad unevenness of
255 the road surface (i.e. on the scale of a few tens to hundreds of millimeters) and has therefore
256 been excluded from this research. Macrotexture displays characteristic dimensions, i.e.
257 deviation of the pavement surface from the local planar surface of the road, in the 0.5-50 mm
258 range; it is determined by means of volumetric sand patch tests carried out at various spots
259 along the tire tracks of the pavement (HK/HD, 1989). The characteristic microtexture
260 dimensions, i.e. defined as the wavelength and amplitude of the cavities and edges on gravel
261 particle surfaces, are less than 0.5 mm (Lowne, 1970; Dahl *et al.*, 2006; Gustafsson *et al.*,
262 2009). Microtexture relates to the microscopic morphology, crystallographic characteristics
263 and chemical composition of both the asphalt concrete and the deposited dust; it is assessed in
264 arbitrary friction units (i.e. a.u.) using a standard skid resistance tester (HK/HD, 1989). Both
265 the micro and macrotexture of the test track pavements are evaluated annually; their relevant
266 values are listed in Table 1.

267 Six pavement types were used to assess the influence of texture on RoWP emissions; this
268 assessment entailed driving the instrumented vehicle on the test track at a speed of 50 km/h.
269 Of the pavements tested, three were also used to determine TRWP emissions. To improve
270 data representativeness, the track was not previously cleaned from ambient dust deposition.
271 Each pavement tested was selected according to its representativeness or due to its distinct
272 micro and macrotexture properties; these pavements consisted of either asphalt concrete (AC),
273 stone mastic asphalt (SMA) or surface dressing (SD) (Table 1). The SMA was a gap-graded
274 mineral mixture with a coarse deformation-resistant aggregate matrix. The matrix was filled

275 with bitumen, mastic and several stabilizing additives. Surface dressings were prepared by
276 spreading a hot bituminous binder onto an existing pavement, then uniformly distributing and
277 sealing the aggregates. This technique usually resulted in increasing both noise emissions and
278 road surface macrotexture. In addition to experiments designed to evaluate the role played by
279 texture, the influence of pavement aging was also examined by driving at constant speeds
280 within the 50-110 km/h interval on two semi-coarse asphalt concrete pavements, 11 (AC₂₀₀₆)
281 and 37 (AC₁₉₈₀) years old respectively at the time of the experiments.

282 All tests were conducted by the same pilot and co-pilot. Beyond the key parameters recorded
283 by on-board computers, the co-pilot logged for each test the vehicle activity and driving
284 conditions. Tests were carried out under dry weather conditions (T = 20-25°C with 50%-80%
285 humidity) and in the absence of any notable wind (less than 5 m/s). Background particles
286 were measured when the vehicle was stationary and facing the wind or running at speeds
287 below 10 km/h (i.e. with emissions from the instrumented vehicle becoming negligible). The
288 background was then manually subtracted for each particle fraction before any type of data
289 processing. To do this, we used a moving average (taken over 20-40 min). This allowed us to
290 adjust the baseline of the signal as well as its variations without significantly altering the
291 superimposed structures. The quality of the adjustment was checked by making sure that the
292 average values correspond to the punctual measurements. Potential contamination by “fresh”
293 brake wear particle (BWP) emissions was also assessed by simultaneously monitoring
294 emissions at the rear and in the backspace (i.e. 15 cm below and 12 cm downstream of the
295 braking system) of the instrumented wheel. Because of the differences among vehicles in the
296 positioning of the braking system and the configuration of the wheel backspace, these
297 distances could vary in a sensible way (from 5 cm to 10 cm). Nevertheless, care has been
298 taken to ensure that the overall configuration and aerodynamics remain relatively consistent
299 (including the position of the air intake in relation to that of the braking system and other
300 internal parts such as the steel beams). The resultant signals and associated size distributions
301 showed that contamination with BWP cannot be excluded during situations where the vehicle
302 comes to a stop after heavy braking (between 8% and 27% of RoWP). In other cases, the
303 majority of BWP emissions were incorporated into the resuspended dust cloud and then
304 discharged downstream of the vehicle without quantitatively reaching the air intake for
305 RoWP.

306 **2.4 On-road RoWP measurements**

307 The on-road measurement campaign was intended to identify and evaluate the determinants of
308 RoWP and TRWP emission dynamics under various driving conditions. The route driven was
309 a 25-km long loop in the Nantes metropolitan area (northwestern France), which encompasses
310 a population of nearly 950,000. The area's vehicle count reached 350,000 in 2016, with traffic
311 being busiest in remote suburban locations (over 100,000 vehicles per day on certain ring road
312 sections) or else in the city core (AURAN, 2016; DREAL, 2016). The tested route passed
313 through different environments, from rural sectors to suburban and urban districts, and
314 covered several road types (i.e. country roads, ring roads, motorways, city streets, speed-
315 limited streets), thus involving a range of traffic situations (e.g. stops at traffic lights,
316 navigating roundabouts, passing junctions, etc.). The atmospheric blanks were determined for
317 each road type by applying the same procedure as described for the measurements on the
318 test track.

319 In order to both maintain a low contribution of exhaust particles from ambient road traffic and
320 increase the consistency of traffic conditions, on-road measurements were carried out between
321 11 am and 5 pm while taking care to avoid the noon rush hour. Traffic conditions were
322 recorded manually by the co-pilot as well as using an on-board camera. The camera was used
323 to search for the causes of variations in emission signals in relation to the zone traveled. The
324 information obtained was qualified according to the operator's interpretation when the vehicle
325 was returned to the laboratory. Although heavy-traffic situations cannot always be avoided in
326 urban zones, these measurements allowed the RoWP and TRWP emission dynamics to be
327 examined over a wide range of speeds: from 0 km/h (i.e. the vehicle was stopped) to over 90
328 km/h. Depending on traffic conditions and analyzer response, one or two successive runs may
329 have been required to compile complete datasets. As with measurements conducted on the test
330 track, most trips took place under the same weather conditions: clear skies with light wind
331 (wind speed below 7 m/s) and no rain during the entire previous week. The air temperature
332 and relative humidity ranged from 10°C to 20°C and from 50% to 90%, respectively. These
333 conditions should prevent hygroscopic particle growth and potential droplet formation that
334 could affect the response of OPCs at humidity percentages close to 100% (Hänel, 1972; Hegg
335 et al., 1993). In addition to weather and traffic conditions, the co-pilot also manually recorded
336 the apparent characteristics of the road surface (i.e. macrotexture, dryness or contamination of
337 dust).

338

339 **3. Results and discussion**

3.1 Determinants of RoWP emission dynamics on the road

It was generally acknowledged that the driving speed factor can decisively alter the dynamics of RoWP emissions. The data obtained from on-road measurements with different vehicles confirmed this assertion (Appendix 3) while nuancing it at the same time. As was the case in the study by Mathissen *et al.* (2011), the slope-to-intercept ratios for the curves plotting total concentration measured in number or mass by the ELPI device (namely $C_{ELPI}(RoWP)$) vs. driving speed were low (i.e. less than 0.01, Fig. S2). In contrast, in considering the average $C_{ELPI}(RoWP)$ values of sections traveled at constant speed, exponential increases ($r^2 > 0.90$) were found above 70 km/h. Such correlations were identified despite a significant increase in the dilution rate, thus highlighting that ELPI RoWP emissions (hereinafter referred to as $E_{ELPI}(RoWP)$) per unit of time intensify with driving speed (Fig. 2). An estimation indicated that RoWP emissions for the instrumented wheel were close to 10^9 particles/s (or 0.05 mg/s) at 90 km/h, and their magnitude was approximated using the least-square regression model with the following power trends:

$$E_{ELPI}(RoWP) \text{ (particles/s)} = 4.0 \cdot 10^6 v^{1.22}; r^2 = 0.70, p < 0.01 \quad \text{(Equation 3a)}$$

$$E_{ELPI}(RoWP) \text{ (mg/s)} = 5.8 \cdot 10^{-4} v^{1.04}; r^2 = 0.60, p < 0.01 \quad \text{(Equation 3b)}$$

where “v” denotes the driving speed in km/h. These relationships incorporate the changes in both the airflow velocity and orientation of streamlines arising from the tire-road interface with changes in driving speed. However, they should only be considered as indicative as most RoWP were induced by resuspension (see Section 3.2), and a significant percentage of emissions was potentially aged RoWP deposited on the pavement and then re-emitted a variable number of times. In addition, turbulence and particulate emissions from road traffic were more likely to affect the concentration and size distribution of RoWP recorded at low speeds. Most RoWP were in the $< 0.1 \mu\text{m}$ range by number and $0.05\text{-}0.40 \mu\text{m}$ or $1.0\text{-}10 \mu\text{m}$ by mass, i.e. roughly 90% and 80%, respectively. It should also be noted that relatively constant evolutions ($r^2 < 0.10$) were found when expressing $E_{ELPI}(RoWP)$ values per kilometer and plotting them vs. driving speed. On the one hand, the limited overall variation in emissions per kilometer could be explained by a quasi-linear increase of temporal emissions with speed (Eqs. 3a and b), while on the other hand, the dispersion of individual values stems from local variations in speed-independent factors, e.g. pavement texture, road surface contamination with dust, road traffic intensity.

371 The squared correlation coefficient in Equations 3(a,b) underscores that driving speed could
372 be used to capture a significant part of variations in RoWP emissions. As a consequence,
373 several other speed-dependent parameters (i.e. fuel consumption, engine speed, throttle
374 opening) were positively correlated with the RoWP emission rate per unit of time. However,
375 an analysis of residuals indicates that Equations 3 and 4 (see Section 3.2) should be used with
376 caution. This is mainly due to the fact that the residuals are not normally distributed, but most
377 likely reflect the superposition of two or more Gaussian distributions (Appendix 4). Further
378 analysis shows that due to the diversity of generation and emission processes, the proposed
379 equations would be: i) better suited to estimate continuous (i.e. non-peaked) emissions and ii)
380 less efficient at speeds exceeding 50-70 km/h. The estimates obtained at higher speeds should
381 then be considered as indicative of an order-of-magnitude. Remarkably, no overall correlation
382 could be found with tire temperature, except at low speeds: a significant increase in
383 $E_{ELPI}(RoWP)$ accompanied the rise in tire temperature or drive shaft torque at speeds slower
384 than 5 km/h ($0.07 < r^2 < 0.16$, $p < 0.05$, Fig. S3). This finding most likely reflects a
385 mechanical heating of the tread and particle detachment from the tire and road surface that
386 would have occurred during the first few moments of driving or acceleration (e.g. when
387 starting up the vehicle from a standstill). Particle detachment can be thought of as the removal
388 of weakly bound solids, i.e. including tire parts, metal inclusions and dust fragments; it
389 becomes more prevalent with an increase in: stresses exerted at the interface between tire and
390 road, centrifugal forces on the tire tread and the flow of air around the wheel. Detachment was
391 also evidenced at the initiation of high-speed accelerations by sudden changes in the RoWP
392 emission dynamics in the form of concentration peaks (Fig. 3), despite the absence of a trivial
393 relationship between peak height and acceleration intensity. Most peaks correspond to an
394 increase in the torque exerted on the wheel, in tire temperature as well as in the number
395 concentration of coarse particles within the 0.05-0.25 μm size range and, more markedly,
396 within the 1-10 μm interval (multiplicative factors of 1.1-1.3 and 1.2-2.5, respectively). This
397 interval was consistent with the size of particulate contaminants observed on the tire tread
398 (Fig. 4).

399 Like in the acceleration case study, decelerations were accompanied by sudden increases in
400 $E_{ELPI}(RoWP)$ values. Let's note however that $E_{ELPI}(RoWP)$ is a simple function of neither the
401 pressure exerted on brake pads nor the deceleration rate. For instance, mild braking at 80
402 km/h can generate twice as many particles as heavy braking at 30 km/h. The particulate
403 concentrations recorded during decelerations were among the highest, i.e. close to $1.5 \cdot 10^{10}$

404 particles/m³ or 1,000 µg/m³, yielding emission peaks approaching 10⁹ particles/s and 3.5
405 mg/s, respectively. At the same time, the proportion of coarse particles in the emissions was
406 increasing considerably by number: within the size range of 0.05-0.25 µm and, especially,
407 within the 1-15 µm interval (multiplicative factors of 1.1-1.2 and 1.3-7.0, respectively). These
408 ranges are consistent with the BWP sizes reported in the literature (Beji *et al.*, 2020), though
409 the data acquired do indicate a higher proportion of particles larger than a micron. It is
410 therefore likely that emitted particles or particles deposited on the pavement will agglomerate
411 at the tire-road interface during braking. These may grow to a size of several micrometers or
412 fragment in order to form new agglomerates. Braking strength and wheel speed would then
413 partly control the agglomeration dynamics and the emission of the particles formed.

414 The coincidence of braking situations and RoWP emission peaks, as well as the proximity
415 between observed particle sizes during accelerations and decelerations, further suggests that:
416 i) the RoWP measured during decelerations accounted for an excess of BWP; and ii) BWP
417 deposited on the pavement and tire surface were potentially re-emitted during accelerations.
418 According to the Kruskal-Wallis test, the excess is most significant when comparing to
419 particles whose diameter lies close to but outside the BWP size ranges (i.e. up to almost
420 +30%). Re-emission would involve resuspension, detachment and wear processes. The
421 presence, on both the tire tread and surface of the coarsest RoWP, of metal fragments
422 enriched with elements found in brake pads and BWP (i.e. Fe, Ba, Al and Zn) reinforces this
423 hypothesis (Fig. 4). Based on our observations, the existence of composite RoWP, comprising
424 BWP, TWP, pavement wear particles (PWP) and/or other mineral inclusions, was definitely
425 likely; this inquiry would require further research in order to assess environmental stability
426 and toxicity.

427 **3.2 Determinants of TRWP emission dynamics on the road**

428 Strong and meaningful correlations were derived between the number concentrations
429 measured at the rear and in the backspace of the instrumented wheel ($0.40 < r^2 < 0.86$, $p <$
430 0.01). A good level of agreement was also found between size distribution in the intervals
431 typically associated with resuspension particles, i.e. in the nanometric and coarse size ranges.
432 For these reasons and under specified conditions, the particles aspirated in the backspace of
433 the wheel would be representative of the resuspension particles in RoWP emissions. In other
434 words, concentrations recorded at the rear and in the backspace of the instrumented wheel can
435 be associated with the presence and absence of TRWP, respectively. The proportion of TRWP
436 can thus be estimated by subtracting the normalized concentration measured in the backspace

437 of the wheel from that measured at the rear of the tire (Appendix 5). This calculation assumes
438 that residual particles present on the tire tracks of the pavement were refractory and therefore
439 relatively unaffected by the crossing of the instrumented wheel (see below). It was moreover
440 postulated that the influence of the particle detachment process was limited, except in
441 acceleration situations or when driving on heavily dust-contaminated roads. A similar
442 postulate was formulated for BWP contamination during heavy braking situations (see
443 Section 2.3).

444 The TRWP size distribution was mostly bimodal (Fig. 5); emissions mainly fell in the size
445 ranges of $< 0.03 \mu\text{m}$ and $0.05\text{-}0.30 \mu\text{m}$ by number and $0.1\text{-}0.6 \mu\text{m}$ and $1.0\text{-}15 \mu\text{m}$ by mass.
446 When visible, the mass-weighted sub-micron fraction of TRWP was much less prominent
447 than that of RoWP. In the size ranges of the maxima, these two modes made up 5-60% (40%
448 on average) and $< 5\text{-}50\%$ (25% on average) of RoWP emissions, respectively. The PM_{10}
449 TRWP were close to 20% of the PM_{10} RoWP, resulting in individual PM_{10} PWP and PM_{10}
450 TWP emissions of $< 0.1\text{-}150$ (average of 2.5) $\text{mg}/\text{km}/\text{vehicle}$. This calculation assumes that
451 the TWP/PWP ratio is close to unity, i.e. a PM_{10} PWP of 3-8 $\text{mg}/\text{km}/\text{vehicle}$ compared to 2.4-
452 9.0 $\text{mg}/\text{km}/\text{vehicle}$ for TWP (Denier van der Gon *et al.*, 2008; EMEP, 2019). A similar
453 approach has indicated that $\text{PM}_{2.5}$ TRWP would average 18% of the measured $\text{PM}_{2.5}$ RoWP
454 concentrations, thus leading to individual $\text{PM}_{2.5}$ PWP and $\text{PM}_{2.5}$ TWP emissions of $< 0.1\text{-}75$
455 (average of 1.2) $\text{mg}/\text{km}/\text{vehicle}$. Our data lie within the lower limit of the emission factor
456 values available in the literature, which reflects the inability of on-board measurement devices
457 to monitor particles larger than a few tens of micrometers whose contribution by mass is
458 probably quite significant. These data however partly confirmed the results obtained using
459 road simulators, which highlighted that the size distribution of TRWP was most often
460 dominated by nanoparticles ($0.02\text{-}0.09 \mu\text{m}$) (Panko *et al.*, 2009; JRC, 2014; Grigoratos *et al.*,
461 2018). Our measurements further show that the nanoparticles dominated in number for 45-
462 50% of the driving time. Their contribution to TRWP emissions increased with time, while
463 the ratio of $< 0.03 \mu\text{m}$ to $0.05\text{-}0.30 \mu\text{m}$ size categories decreased with tire temperature ($0.14 <$
464 $r^2 < 0.25$, $p < 0.01$). This finding suggests that the categories $\text{TRWP}_{<0.03\mu\text{m}}$ and $\text{TRWP}_{0.05\text{-}$
465 $0.30\mu\text{m}}$ would originate from distinct sources or mechanisms, e.g. the repeated wear of
466 contaminants that continuously accumulate on the tire tread or the primary emission of
467 abraded particles at the tire-road interface.

468 To refine these results, the influence of driving conditions on TRWP emissions was examined
469 for road sections where $|\text{dv}/\text{dt}|$ was less than $0.2 \text{ m}/\text{s}^2$ and speed remained in the 30-90 km/h

470 interval. Assuming that the TWP/PWP ratio lies close to unity, then $E_{ELPI}(TWP)$ by mass and
471 per kilometer would barely increase with speed or exceed the mass loss specified by the tire
472 manufacturer: 20 mg/km/vehicle. In fact, the $E_{ELPI}(TWP)$ averages ranged from 2 to 3 mg per
473 kilometer per vehicle, yet individual values varied widely within a range of 0.08 to 20
474 mg/km/vehicle. This limited increase nevertheless indicates a moderate intensification of tire
475 and/or pavement wear mechanisms with speed, thus making high-speed road sections
476 preferred sites for atmospheric air mass contamination with TRWP. In contrast with the
477 emissions per mass and per kilometer, $E_{ELPI}(TRWP)$ values per second increased significantly
478 with driving speed (Fig. 2). The values calculated for the instrumented wheel were fitted by
479 the following relationships:

480
$$E_{ELPI}(TRWP) \text{ (particles/s)} = 9.1 \cdot 10^5 v^{1.26}; r^2 = 0.84, p < 0.01 \quad \text{(Equation 4a)}$$

481
$$E_{ELPI}(TRWP) \text{ (mg/s)} = 2.1 \cdot 10^{-4} v^{1.18}; r^2 = 0.72, p < 0.01 \quad \text{(Equation 4b)}$$

482 It logically follows that under specified conditions, the proportion of TRWP in number-
483 weighted RoWP emissions is either relatively constant or gradually increases with speed.
484 These proportions were calculated at 26%-27% by number and 57%, 61%, 64% and 66% by
485 mass at 30 km/h, 50 km/h, 70 km/h and 90 km/h, in this order. The correlation coefficient
486 indicates that driving speed could be the main factor responsible for the recorded variations in
487 $E_{ELPI}(TRWP)$ values. At high speeds, the smaller contribution of particles resulting from
488 resuspension can be explained by both the intensification of wear mechanisms (most likely of
489 the tire tread) and a lower degree of pavement dust contamination. While the former process
490 would seem to prevail (Wong, 2001; Manas *et al.*, 2009), the effect of the latter cannot be
491 minimized (Thorpe *et al.*, 2007). Compared to the hard shoulder of the motorway, the gravel
492 making up the tire tracks actually revealed fewer particle deposits and smaller particle sizes
493 (i.e. Fig. S4; Changarnier *et al.*, 2018). These less numerous particle deposits were often
494 optically opaque, which suggests a greater content of high atomic number elements. The
495 coarser particles initially present on the gravel would have been caught at high speed on the
496 vehicle's tire tread, mixed with adjacent materials or else broken into smaller pieces. The
497 fragments would have been carried away by the induced heterogeneous turbulence, thus
498 enhancing the apparent contribution of wear particles. The importance of this observation lies
499 in the fact that the remaining particulate contaminants can act as a third body (i.e. wear
500 particles whose mechanical behavior and chemical composition contrast significantly with
501 those of the materials initially brought into contact) altering the TRWP production
502 mechanism. In contrast to tire sidewalls or grooves, a multitude of metal fragments and

503 mineral inclusions along the tread were found as sources of local punctures or tears (Fig. 4),
504 which implies that reducing TRWP emissions requires measures adapted to the driving speed
505 as well as to the degree and composition of road contamination. Such measures may include
506 more frequent sweeping or vacuuming of city streets and suburban roads, plus the
507 implementation of wear-resistant materials for tires and high-speed road pavements. In
508 addition, above 70 km/h, a limited decrease in both maximum driving speed and the
509 magnitude of speed variations can significantly lower RoWP and TRWP emission rates.

510 Among other factors capable of affecting TRWP emission rates, the influence of tire
511 temperature and road slope was specifically evaluated. As was the case for RoWP,
512 $E_{ELPI}(TRWP)$ per second increased with tire temperature and drive shaft torque at speeds
513 below 5 km/h ($0.12 < r^2 < 0.14$, $p < 0.05$, Fig. S3) and, more episodically, at the start of the
514 highest accelerations (Fig. 3). This finding suggests that the detachment of particulate
515 contaminants from the pavement and tire tread (see the previous paragraph and Section 3.1)
516 could also affect TRWP emission through generation of a third body promoting pavement
517 abrasion and/or point tears in the tire tread. With regard to the influence of road slope, all
518 measurements were carried out at speeds between 55 km/h and 65 km/h. Data show that
519 TRWP emissions exhibit higher percentages of particles smaller than $0.03 \mu\text{m}$ when climbing
520 or descending 5-8% slopes. These increases (between 60% and 90% by number) were
521 recorded to the detriment of $0.05\text{-}0.30 \mu\text{m}$ particles (between -15% and -25%), thus
522 indicating that high-speed driving on steep roads can alter the TRWP size distribution in a
523 way that favors the emission of nanometric particles. Moreover, the percentage of
524 micrometric TRWP above $3 \mu\text{m}$ also increased when climbing or braking during descents.
525 Recorded changes in the size distribution suggest: i) development of the abrasion mechanisms
526 more toward the depth of the tire tread and/or road surface; ii) establishment of particle
527 agglomeration mechanisms (see Section 3.1) or ii) contamination by coarse particles
528 (including BWP) from the vehicle or surrounding road traffic.

529 **3.3 Spatial distribution of emissions in relation to the areas being crossed**

530 Previous studies have pointed out that urban driving is often associated with higher wear per
531 kilometer. Accordingly, more tire tread and asphalt are being lost during acceleration, braking
532 and cornering, and the amount of material lost would thus tend to be greater near heavily-
533 trafficked junctions and on road bends. The ELPI data locally contradicted this assertion
534 because both number- and mass-weighted RoWP and TRWP emissions could be significantly
535 lower in urban areas than in the remainder of the crossed areas ($p < 0.05$, Fig. 5), except for

536 remote suburban roads (i.e. close to the metropolitan fringe). This finding primarily reflects
537 the lower driving speeds and numerous idling periods associated with urban driving. The
538 limited emissions for remote suburban roads can be explained by a combination of moderate
539 speeds (around 50 km/h) and frequent sweeping or vacuuming of the pavement. This
540 reasoning equally applies to more centrally located suburban roads. However, due to the
541 increase in road traffic, both exhaust and locally re-suspended particles were more likely to be
542 superimposed on RoWP and TRWP vehicle emissions. In fact, compared to data from remote
543 suburban locations, RoWP and TRWP emissions in more central suburban areas exhibit
544 higher proportions of particles smaller than 0.03 μm or larger than 1.0 μm .

545 As could be expected, the highest emissions were recorded on the motorway or country roads.
546 Their ELPI-averaged emissions exceeded the values for city streets, suburban and ring roads
547 by factors of 3-12 and 2-21, 2-18 and 6-10, and 2-4 and 2-5 by number and mass for RoWP
548 and 4-20 and 2-24, 3-14 and 2-8, and 3-6 and 2-6 by number and mass for TRWP,
549 respectively. The overall disparity increases not only with the difference in driving speed but
550 also with the degree of apparent road surface dust contamination. Country roads and
551 motorways were more prone to increased particulate deposition from adjacent industrial
552 facilities or agricultural activities. The influence of pavement dust contamination was
553 evaluated by comparing the emissions from uncontaminated and contaminated lanes of the
554 same motorway section located near a stone quarry exit (items numbered 1 and 3 in the upper
555 panels of Fig. 5). This evaluation was carried out after correcting for the speed difference, i.e.
556 less than 10 km/h. On the one hand, at 80-90 km/h, $E_{\text{ELPI}}(\text{RoWP})$ and $E_{\text{ELPI}}(\text{TRWP})$ values
557 increased by factors of 0.5-2.4 (average: 1.2) and 0.7-2.6 (average: 1.7), respectively. Yet on
558 the other hand, OPC data show a sharp increase in coarse RoWP and TRWP emissions, i.e. by
559 factors of 2.4-5.6 (average: 3.9) and 1.2-4.5 (average: 2.6), respectively. Increases were most
560 pronounced for particles larger than one micron, particularly in the 1-5 μm size range:
561 multiplicative factors of 1.9-7.2 (average: 4.9). The data overall suggest that the mobilizable
562 fraction of particulate contaminants less than one micrometer in diameter was likely small.
563 Put otherwise, although micrometric dust particles were readily driven off, the persistence of a
564 third body (probably made up of refractory, i.e. hardly mobilizable, submicron particles)
565 considerably increased the wear of both pavement and tire tread. The presence of refractory
566 contaminants in the form of submicron particles was corroborated by microscopic
567 observations showing the smaller diameter of dust aggregates deposited on the gravel
568 constituting the tire track surface (see Section 3.2). It is worth noting that regular pavement

569 cleaning would have the benefit of limiting emissions of both RoWP and TRWP. However,
570 since a notable share of the submicron particles deposited on the pavement was due to wear
571 processes, it is likely that TRWP emissions will progressively intensify after cleaning until a
572 new equilibrium state has been reached.

573 Extending this line of investigation further, the magnitude of RoWP and TRWP emissions
574 was probed for various structural elements and equipment affecting road traffic (bar charts in
575 Fig. 5). The data show that total emissions were highest for high-grade bridges, followed by
576 heavily-trafficked junctions or large roundabouts (items numbered 1, 2 and 4 in the bar charts,
577 lower panels of Fig. 5). Depending on the data weighting, the difference in relative emissions
578 for the last two structures and the entire route was not always significant at the 0.05
579 confidence level. This observation suggests that the dynamics of RoWP and TRWP emissions
580 would be more sensitive to road slope than to steering angle. However, the role of the steering
581 angle should not be overlooked, as emissions increase significantly when cornering at 25-35
582 km/h. As regards RoWP, the multiplicative factors for the widest (i.e. steering angle below 40
583 degrees) and tightest (steering angle exceeding 40 degrees) corners were in the 1.4-3.1
584 (average: 2.1) and 1.7-3.7 (average: 2.8) ranges, respectively. The corresponding TRWP
585 values were 1.5-2.1 (average: 1.8) and 1.4-3.5 (average: 2.6). The data have been corrected
586 for the difference in driving speed with respect to steering angle. The increase was fairly
587 consistent across RoWP size classes, which means that cornering did not substantially modify
588 the shape of their size distribution curves. This reasoning is also partly true for TRWP
589 emissions, except for particles $< 0.03 \mu\text{m}$, which exhibited a stronger increase of their
590 number-weighted contribution: multiplicative factors for the widest and tightest corners of
591 2.6 ± 0.7 and 7 ± 2 , respectively. Moreover, the lowest emissions were typically found for
592 structures with driving either at significantly reduced speed or stopped, i.e. small roundabouts
593 or traffic lights. The latter case however was depicted by increased contamination in the
594 exhaust particle size range during startup. Once again, the data underscore the central role
595 played by speed in controlling RoWP and TRWP emissions and, consequently, the potential
596 benefits of structural elements that reduce speed without disrupting traffic flow.

597 **3.4 Assessment of RoWP emission dynamics on the test track**

598 Results on the influence of speed and its variation on RoWP emissions have been published in
599 another paper (Beji *et al.*, 2020); they confirmed that RoWP emissions on the test track were
600 mostly in the $< 0.1 \mu\text{m}$ range by number, with an accumulation mode centered at 0.2-0.3 μm
601 and a major coarse mode centered at 2-4 μm by mass. The data show a strong increase in

602 emissions at higher speeds and during the most intense accelerations. Regarding
 603 decelerations, RoWP emissions increased with both braking intensity and speed at the start of
 604 braking. The strongest accelerations ($> 2.50 \text{ m/s}^2$) favored the production of particles smaller
 605 than $0.1 \text{ }\mu\text{m}$, while higher speeds and heavy high-speed decelerations increased the rate of
 606 coarse particles. All these observations were consistent with the data obtained from on-road
 607 measurements. However, on-road measurements were unable to give access to the RoWP
 608 emissions associated with the most extreme accelerations and decelerations and, therefore, to
 609 nano- and micrometric particles associated with more intense road dust fragmentation or
 610 pavement and tire wear at higher temperature.

611 Another advantage of test track measurements is the possibility of assessing the influence of
 612 pavement texture (Table 1) on the RoWP emission rate (Fig. 6). At a speed of 50 km/h , the
 613 relative ELPI RoWP concentration (i.e. divided by the average concentration measured on
 614 AC2 pavement and after background subtraction) decreased linearly with increasing
 615 microtexture (Eq. 5).

$$616 \quad R_{\text{RoWP}} = -1.3 R_{\text{MicTex}} + 2.1; r^2 = 0.90, p < 0.05 \quad (\text{Equation 5})$$

617 where R_{RoWP} denotes the ratio of the average RoWP concentration measured on the pavement
 618 to that of the AC2 pavement, and R_{MicTex} (resp. R_{MacTex}) the ratio of the corresponding
 619 micro/macrottexture values. Since the microtexture was assessed using a standard skid
 620 resistance tester, Equation 5 indicates that high microtexture values would improve driving
 621 safety while potentially limiting RoWP emissions. The ratio of the highest relative
 622 concentration (AC3 data) to the lowest (SD1 data) exceeds 7, thus further suggesting that the
 623 decrease in emissions may be large. Alternatively, it implies that traffic-induced pavement
 624 polishing might increase RoWP levels. Whereas the ultrafine particulate concentration
 625 decreases with increasing microtexture, both accumulation and coarse mode RoWP levels
 626 exhibit a bulge-shaped evolution, with maxima observed for AC1 or SMA pavements. These
 627 nonlinear trends demonstrate that additional factors, including macrottexture, deposited dust
 628 quantities and induced air turbulence, play significant roles in RoWP emissions. Except for
 629 the extreme macrottexture values (i.e. for AC1 and/or SD2 pavements), the accumulation and
 630 coarse mode RoWP concentrations do decrease with increasing macrottexture. The decreases
 631 were meaningful, large and closely approximated by the following equations:

$$632 \quad R_{\text{RoWP_ACC}} = -1.3 R_{\text{MacTex}} + 2.5; r^2 = 0.90, p < 0.05 \quad (\text{Equation 6a})$$

$$633 \quad R_{\text{RoWP_CRS}} = 7.3 \exp(-2.0 R_{\text{MacTex}}); r^2 = 0.89, p < 0.05 \quad (\text{Equation 6b})$$

634 where the RoWP_ACC and RoWP_CRS subscripts stand for the accumulation and coarse
635 mode RoWP, respectively. Hence, pavements with a high level of macrotexture would
636 contribute to both an increase in skid resistance and a decrease in fine and micrometric RoWP
637 levels. This result is consistent with data provided by China and James (2012); nonetheless, it
638 proves to be counterintuitive since deep textures would favor tire wear and collection of
639 emissions, then the partial re-suspension of dust deposited into surface cavities (Lundberg *et*
640 *al.*, 2017; Blomqvist *et al.*, 2013). The data obtained therefore need to be supplemented by
641 microscopic and macroscopic measurements on a wider range of pavements. It is however
642 important to stress that road pavement may be optimized to maintain a high standard of
643 driving safety while improving air quality. This optimization can be achieved by using
644 pavements whose formulations and textures have been adapted to local road traffic and
645 surrounding sources of particulate matter.

646 Lastly, the influence of road pavement aging has been investigated by means of the AC₁₉₈₀
647 and AC₂₀₀₆ pavements. Macrotexture and microtexture values indicate that the AC₁₉₈₀
648 pavement has not yet reached the late stage associated with polished aggregate (Table 1).
649 Instead, it represents an intermediate stage of increased skid resistance. Concentration
650 measurements have indeed shown that this 37-year-old pavement accounts for lower RoWP
651 levels: relative decrease of 5-40% by number. The decrease was less pronounced at low speed
652 for the ultrafine mode, while the decreases in accumulation and coarse mode RoWP
653 concentration were minimal at 70 km/h. This finding highlights that the texture evolution does
654 influence the variation amplitude of fine and micrometric RoWP levels with speed. As a
655 result, the aging effect would be more apparent at speeds above 90 km/h.

656 **3.5 Assessment of TRWP emission dynamics on the test track**

657 The shape of the size distribution curves for TRWP emissions on the test track is similar to
658 that of on-road emissions. Nevertheless, in spite of the fact that all vehicle parts, weather
659 conditions and instrument settings remain unchanged, the mode mean diameters shift to
660 higher values (see item numbered 5, upper panels of Fig. 5). At speeds from 10 to 90 km/h,
661 the number size distribution after background removal was bimodal, with an ultrafine mode
662 centered around 0.03-0.06 μm and a more minor accumulation mode between 0.15 μm and
663 0.5 μm . The mass size distribution was also bimodal, with an accumulation mode centered at
664 1.0 μm and a coarse mode between 4 μm and 15 μm . For purposes of comparison, a unimodal
665 mass size distribution (centered at approx. 4 μm) was observed when using a tire simulator
666 (Gibaek and Seokhwan, 2018). The (coefficient;exponent) vectors associated with Equations

667 4a and 4b were ($4.1 \cdot 10^5$;1.00) and ($9.8 \cdot 10^{-5}$;1.18) for number and mass-weighted TRWP
668 emissions ($r^2 > 0.85$, $p < 0.05$), respectively. Accordingly, the emissions of fine and ultra-fine
669 TRWP on the test track underestimated those determined on the road, especially at high
670 speeds. This result was not surprising since the traffic was limited and the pavement
671 frequently cleaned (by sweeping and vacuuming), hence $E_{ELPI}(RoWP)$ estimates were 7-15%
672 by number and 50-60% by mass of the road measurements. These percentages became 30-
673 70% and 50-60% when considering the OPC data. Test track measurements would therefore
674 better reflect TRWP emissions on roads with low submicron particulate contamination.

675 Like with on-road measurements, concentration peaks were recorded during the first moments
676 of accelerations and at the end of decelerations (Fig. S5). The height of these peaks increases
677 with speed variation in the case of accelerations: by factors of 1.0, 1.2-2.3, 1.9-4.8 and 2.9-7.5
678 at 0.80 m/s^2 (set as the reference), 0.85 m/s^2 , 1.05 m/s^2 and 1.35 m/s^2 , respectively (Fig. 7).
679 Only minor changes in the average mode size were detected. Compared to the size
680 distributions obtained at constant speeds in the 85-90 km/h range however, higher levels of
681 ultrafine and micrometric TRWP were observed during accelerations, e.g. at 1.35 m/s^2 ,
682 multiplicative factors of 6.1-7.8 for ultrafine TRWP and 3.6-7.0 for micrometric TRWP. This
683 finding probably reflected the detachment of particles from the tire and road surface as
684 opposed to any continuous wear processes. As for deceleration, the height of the
685 concentration peaks increases with vehicle speed recorded at the start of braking.
686 Consequently, mild braking at 90 km/h can generate more than twice as much TRWP as
687 heavy braking at 50 km/h. The key conclusion drawn here is that the emission factors for
688 braking situations might be proportional to the kinetic energy of the vehicle (Fig. 7) and
689 therefore to its stopping distance. This conclusion is also consistent with data available in the
690 literature showing that a reduction in vehicle kinetic energy (i.e. the amount of energy to be
691 dissipated) yields less tire wear during braking situations (Janićijević, 2015; Ma *et al.*, 2017).
692 However, the importance of braking force should not be minimized, given that heavier
693 braking at the same speed ($[\times 1.3 - \times 6.3]$ power range) always leads to a higher total TRWP
694 concentration. The resulting multipliers were in the ranges of: 1.3-3.4 and 1.1-2.7 in number
695 and mass, respectively. With respect to vehicle speed or kinetic energy, the maximum
696 increase in peak height is observed for an increase in braking power by a factor of 3-4. This
697 means that wear mechanisms would be less effective during the initial and terminal stages of
698 heavy braking, i.e. when the variation in braking power most pronounced. Moreover, the size
699 distribution was similar to that of acceleration, i.e. higher percentages by number of

700 nanometric and ultrafine particles than those determined at stabilized speeds. The percentage
701 of particles smaller than 0.1 μm increased on the whole with the height of concentration
702 peaks, probably due to the combined emissions of ultrafine particles and readily condensing
703 volatile organic compounds. An added contribution of coarse particles (centered at 6 μm) was
704 also observed during the heaviest decelerations, possibly reflecting the plume of particles
705 mobilized in the wake of the tire or vehicle body.

706 The influence of road pavement aging on TRWP emissions has been examined by comparing
707 data for AC₁₉₈₀ and AC₂₀₀₆ pavements. At constant speeds of 50 km/h or 90 km/h, no
708 significant differences were identified between the emission factors or size distributions for
709 both pavements, suggesting that under these specified conditions, the TRWP emission
710 mechanism was less sensitive to changes in texture properties than that of RoWP. The
711 significance of pavement type was nevertheless considerable. For instance, the number-
712 weighted emission of ultrafine TRWP on a SMA pavement was 50-70% lower than that of
713 AC pavements, which may be reflective of the original purpose during the mid-1960's of
714 designing SMA pavements as a wearing course with particularly high resistance to studded
715 tires (Drüschner and Schäfer, 2005). Because of the limited amount of data, it is unclear
716 however whether this lower emission resulted from the mixture composition, pavement
717 texture or a combination of both.

718

719 **4. Conclusion**

720 For a given combination of pavement, tire and vehicle type, RoWP and TRWP emissions
721 were shown to be highly dependent on driving speed. This result, although intuitive, paves the
722 way for developing calculation tools to estimate the emission of these two particle categories
723 during a vehicle trip. However, an accurate assessment (i.e. on the order of 10%) is not easily
724 achievable due to the variety of factors altering the relationship with speed, including
725 pavement and tire composition and texture, road surface contamination with mineral dust and
726 wear particles, road traffic characteristics, and driver behavior. In addition, low-cost dust
727 monitors could be mounted in vehicles to detect high emission situations and alert the driver
728 to reduce driving speed.

729 A key result was the predominant share of nanoparticles and ultrafine particles in number-
730 weighted RoWP emissions. A significant share of the ultrafine RoWP emissions stemmed
731 from abrasion processes, which participated in the constitution of a third body that amplified

732 TRWP emissions. It would therefore seem that TRWP emission dynamics partly reflect the
733 state of equilibrium between the accumulation of this third body and its discharge. This
734 distinctly dynamic process would involve the agglomeration and successive recycling of
735 particulate deposits, present on tires and the road surface, applied to a variety of particles,
736 including metal particles released during braking, and involving several mechanisms, e.g. the
737 detachment of particles trapped on the tire during acceleration. This result prefigures the
738 emerging problem of composite particles, whose components stem from braking, tire or road
739 wear processes; it also prompts us to further examine their toxicity and determine whether
740 they can collect and convey exhaust emissions.

741 The actual location and extent of health and environmental problems caused by RoWP and
742 TRWP emissions remain largely unknown. This statement is especially true given that our
743 results challenge the commonly accepted position of the most highly-emitting situations.
744 Urban cores would not be the most conducive to these emissions, but instead suburban areas
745 where road surface particle contamination, traffic speed and its variations were all more
746 pronounced. Nevertheless, let's point out that a decrease in speed below 70 km/h, smoother
747 traffic flow and frequent pavement cleaning would contribute to a significant reduction in
748 both types of emissions. Optimized tires and/or adapted pavements, milder slopes, structural
749 elements and road equipment affecting traffic can supplement this reduction as well.

750 In closing, despite the obvious contrast in emission rates of both RoWP and TRWP, test track
751 measurements do appear to be a valuable source of information. The limitations encountered
752 were due to differences in traffic flow and pavement cleaning frequency. However, in the
753 future, these limitations will also make it possible to study in detail the role of road surface
754 contaminants and the third body in TRWP generation and dust re-emission. Those will
755 equally yield access to a controlled evaluation of how pavement texture and aging affect the
756 wear mechanisms developing at the tire-road interface. The data obtained so far indicates that
757 higher micro and macrottexture values would result in lower RoWP emissions while
758 enhancing driving safety. This result would not readily apply to TRWP emissions since the
759 nature of the mix materials used in the pavement would also play a specific role. Further
760 research is needed in order to objectify this hypothesis and, as a long-term objective,
761 determine the potential link between noise and particulate emissions.

762

763 **Acknowledgments**

764 This study was funded by ADEME (French Environment and Energy Management Agency)
765 through the “Physical Characterization of the Non-Exhaust Particle Emissions by Road
766 Vehicles” project (or Captatus) (grant number: 1566C0016). In particular, the authors
767 gratefully acknowledge L. Gagnepain with ADEME for fruitful scientific exchanges and
768 would like to thank L. Suard, S. Louis, A. Guilloux and S. Buisson for their assistance in
769 setting up the test track experiments and ensuring vehicle availability. Authors finally
770 acknowledge R. Sachs who edited the transcript and the constructive comments by three
771 anonymous reviewers.

772 **References**

- 773 Abu-Allaban M., Gillies J.A., Gertler A.W., Clayton R., Proffitt D. (2003). Tailpipe, resuspended road
774 dust, and brake-wear emission factors from on-road vehicles. *Atmospheric Environment*, 37:
775 5283-5293.
- 776 Amato F. (2018). *Non-exhaust emissions: An urban air quality problem for public health; impact and*
777 *mitigation measures*. Academic Press, Elsevier Inc., 330pp. ISBN 978-0-12-811770-5.
- 778 AURAN (2016) Territorial dynamics in the Nantes metropolis. Report in French on the large area
779 displacement survey under contracting authority of CD44, Nantes Métropole, CARENE, CAP
780 Atlantique. 7pp. [https://www.data.gouv.fr/fr/datasets/enquete-deplacements-en-loire-atlantique-](https://www.data.gouv.fr/fr/datasets/enquete-deplacements-en-loire-atlantique-2/)
781 [2/](https://www.data.gouv.fr/fr/datasets/enquete-deplacements-en-loire-atlantique-2/) (07/2020)
- 782 Beji A., Deboudt K., Khardi S., Muresan B., Flament P., Fourmentin M., Lumière L. (2020). Non-
783 exhaust particle emissions under various driving conditions: Implications for sustainable
784 mobility. *Transportation Research Part D Transport and Environment*, 81: 102290.
785 <https://doi.org/10.1016/j.trd.2020.102290>
- 786 Belyaev S.P., Levin L.M. (1974). Techniques for collection of representative aerosol samples. *Journal*
787 *of Aerosol Science*, 5: 325-338.
- 788 Blau P.J. (2001). *Compositions, functions, and testing of friction brake materials and their additives*.
789 *Oak Ridge National Laboratory Report, ORNL/TM-2001/64* 23pp. Tennessee (USA).
- 790 Blomqvist G., Gustafsson M., Lundberg T. (2013). Road surface dust load is dependent on road
791 surface macro texture. *European Aerosol Conference, Prague, Czech Republic (EU)*.
- 792 Bukowiecki N., Lienemann P., Hill M., Furger M., Richard A., Amato F., Prévô A.S.H., Baltensperger
793 U., Buchmann B., Gehrig R. (2010). PM10 emission factors for non-exhaust particles generated
794 by road traffic in an urban street canyon and along a freeway in Switzerland. *Atmospheric*
795 *Environment*, 44: 2330-2340. <https://doi.org/10.1016/j.atmosenv.2010.03.039>
- 796 Camatini M., Crosta G.F., Dolukhanyan T., Sung C., Giuliani G., Corbetta G.M., Cencetti S.,
797 Regazzoni C. (2001). Microcharacterization and identification of tire debris in heterogeneous
798 laboratory and environmental specimens. *Materials Characterization*, 46(4): 271-283. doi:
799 10.1016/S1044-5803(00)00098-X
- 800 Changarnier S., Hichri Y., Cerezo V., Do M.T., Salvatore F., Zahouani H. (2018). Observations of dry
801 particles behaviour at the tyre/road interface. *Tribology International*, 291–301.
802 <https://doi.org/10.1016/j.triboint.2018.07.023>
- 803 Charron A., Polo-Rehn L., Besombes J.-L., Golly B., Buisson C., Chanut H., Marchand N., Guillaud
804 G., Jaffrezo J.-L. (2019). Identification and quantification of particulate tracers of exhaust and
805 non-exhaust vehicle emissions. *Atmospheric Chemistry and Physics*, 19: 5187–5207.
806 <https://doi.org/10.5194/acp-19-5187-2019>
- 807 China S., James D.E. (2012). Influence of pavement macrotexture on PM10 emissions from paved
808 roads: A controlled study. *Atmospheric Environment*, 63: 313–326.
809 <https://doi.org/10.1016/j.atmosenv.2012.09.018>.
- 810 Dahl A., Gharibi A., Swietlicki E., Gudmundsson A., Bohgard M., Ljungman A., Blomqvist G.,
811 Gustafsson M. (2006). Traffic-generated emissions of ultrafine particles from pavement–tire
812 interface. *Atmospheric Environment*, 40(7): 1314–23.
813 <https://doi.org/10.1016/j.atmosenv.2005.10.029>.
- 814 Denier van der Gon H., Broeke H.T., Hulskotte J. (2008). Emissies door wegdekslijtage ten gevolge
815 van het wegverkeer. Research report in Dutch 17pp. TNO, Nederland (EU).
816 <http://www.emissieregistratie.nl/erpubliek/misc/documenten.aspx>. (June 2020)
- 817 DREAL (2016). The Nantes ring road stakes & projects. Press file release. Report number 844 in
818 French 15 pp.
819 [https://www.prefectures-regions.gouv.fr/pays-de-la-loire/Documents-publications/Salle-de-](https://www.prefectures-regions.gouv.fr/pays-de-la-loire/Documents-publications/Salle-de-presse/Dossiers-de-presse/2016/Le-peripherique-de-Nantes-enjeux-projets)
820 [presse/Dossiers-de-presse/2016/Le-peripherique-de-Nantes-enjeux-projets](https://www.prefectures-regions.gouv.fr/pays-de-la-loire/Documents-publications/Salle-de-presse/Dossiers-de-presse/2016/Le-peripherique-de-Nantes-enjeux-projets) (07/2020)
- 821 Drüschner L., Schäfer V. (2005). Stone mastic asphalt. Asphalt guide. German asphalt association 31
822 pp. Germany (EU).
- 823 ECA (2019). The EU’s response to the “dieselgate” scandal” European Court of Auditions. Briefing
824 paper report 48pp. Luxembourg (EU).

825 [https://www.eca.europa.eu/lists/ecadocuments/brp_vehicle_emissions/brp_vehicle_emissions_e](https://www.eca.europa.eu/lists/ecadocuments/brp_vehicle_emissions/brp_vehicle_emissions_en.pdf)
826 [n.pdf](https://www.eca.europa.eu/lists/ecadocuments/brp_vehicle_emissions/brp_vehicle_emissions_en.pdf) (may 2019)

827 EEA (2016). Explaining road transport emissions. A non-technical guide. European Environment
828 Agency. Report 54pp. Copenhagen, EU. ISBN: 978-92-9213-723-6.
829 <https://www.eea.europa.eu/publications/explaining-road-transport-emissions> (may 2019).

830 Etyemezian V., Kuhns H., Gillies J., Chow J., Hendrickson K., McGown M., Pitchford M. (2003).
831 Vehicle-based road dust emission measurement (III): Effect of speed, traffic volume, location,
832 and season on PM10 road dust emissions in the Treasure Valley. *Atmospheric Environment*,
833 37(32): 4583–4593.

834 EMEP (2019). 1.A.3.b.vi Road transport: Automobile tyre and brake wear. 1.A.3.b.vii Road transport:
835 Automobile road abrasion. Air pollutant emission inventory guidebook 32 pp.
836 [https://www.eea.europa.eu/publications/emep-eea-guidebook-2016/part-b-sectoral-guidance-](https://www.eea.europa.eu/publications/emep-eea-guidebook-2016/part-b-sectoral-guidance-chapters/1-energy/1-a-combustion/1-a-3-b-vi/view)
837 [chapters/1-energy/1-a-combustion/1-a-3-b-vi/view](https://www.eea.europa.eu/publications/emep-eea-guidebook-2016/part-b-sectoral-guidance-chapters/1-energy/1-a-combustion/1-a-3-b-vi/view) (June 2020)

838 Gibaek K., Seokhwan L. (2018). Characteristics of tire wear particles generated by a tire simulator
839 under various driving conditions. *Environmental Science and Technology*, 52(21): 12153–
840 12161. <https://doi.org/10.1021/acs.est.8b03459>.

841 Grigoratos T., Gustafsson M., Eriksson O., Martini G. (2018). Experimental investigation of tread wear
842 and particle emission from tyres with different treadwear marking. *Atmospheric Environment*,
843 182: 200–212.

844 Gustafsson M., Blomqvist G., Gudmundsson A., Dahl A., Jonsson P., Swietlick E. (2009). Factors
845 influencing PM10 emissions from road pavement wear. *Atmospheric Environment, Urban Air*
846 *Quality*, 43(31): 4699–4702. <https://doi.org/10.1016/j.atmosenv.2008.04.028>.

847 Hänel G. (1972). Computation of the extinction of visible radiation by atmospheric aerosol particles as
848 a function of the relative humidity, based upon measured properties. *Journal of Aerosol Science*,
849 3: 377–386.

850 Harrison R.M., Jones A.M., Gietl J., Yin J., Green D.C. (2012). Estimation of the contributions of
851 brake dust, tire wear, and resuspension to non-exhaust traffic particles derived from atmospheric
852 measurements. *Environmental Science and Technology*, 46: 6523-6529.

853 Hegg D., Larson T., Yuen P.F. (1993). A theoretical study of the effect of relative humidity on light
854 scattering by tropospheric aerosols. *Journal of Geophysical Research: Atmospheres*, 98: 18435–
855 18439.

856 Hichri Y. (2019). Skid resistance of particle-contaminated pavements. Ph. D. Thesis (in French) of the
857 Loire Bretagne University 224pp. <http://www.theses.fr/2018ECDN0024> (07/2020)

858 HK/HD (1989). Guidance notes on road testing: (i) Permeability test, (ii) Sand patch test, (iii) Skid
859 resistance test, (iv) Surface irregularity test, (v) Benkleman beam deflection test. Technical note
860 by the Highway Department R&D division 41pp. Hong Kong, CN.
861 [https://www.hyd.gov.hk/en/publications_and_publicity/publications/technical_document/guidan](https://www.hyd.gov.hk/en/publications_and_publicity/publications/technical_document/guidance_notes/index.html)
862 [ce_notes/index.html](https://www.hyd.gov.hk/en/publications_and_publicity/publications/technical_document/guidance_notes/index.html) (may 2019)

863 ICCT (2017). From laboratory to road. A comparison of official and 'real-world' fuel consumption and
864 CO2 values for cars in Europe and the United States, China, and Japan. International Council on
865 Clean Transportation. White paper report 60pp. Germany (EU).
866 <https://theicct.org/publications/laboratory-road-intl> (may 2020)

867 Janićijević N. (2015). Tyre wear during braking. *Journal of Applied engineering Science*, 13(3): 321,
868 137-140.

869 JRC (2014). Non-exhaust traffic related emissions_Brake and tyre wear PM. Literature review 53pp.
870 JRC Science and policy reports, Luxembourg (EU). ISBN 978-92-79-38302-1
871 [https://ec.europa.eu/jrc/en/publication/eur-scientific-and-technical-research-reports/non-](https://ec.europa.eu/jrc/en/publication/eur-scientific-and-technical-research-reports/non-exhaust-traffic-related-emissions-brake-and-tyre-wear-pm)
872 [exhaust-traffic-related-emissions-brake-and-tyre-wear-pm](https://ec.europa.eu/jrc/en/publication/eur-scientific-and-technical-research-reports/non-exhaust-traffic-related-emissions-brake-and-tyre-wear-pm) (July 2020)

873 Ketzler M., Omstedt G., Johansson C., Düring I., Pohjolar M., Oetl D., Gidhagen L., Wahlin P.,
874 Lohmeyer A., Haakana M., Berkowicz R. (2007). Estimation and validation of PM2.5/PM10
875 exhaust and non-exhaust emission factors for practical street pollution modeling. *Atmospheric*
876 *Environment*, 41: 9370-9385.

877 Klöckner P., Reemtsma T., Eisentraut P., Braun U., Ruhl A.S., Wagner S. (2019). Tire and road wear
878 particles in road environment – Quantification and assessment of particle dynamics by Zn

determination after density separation. *Chemosphere*, 222: 714-721. doi: 10.1016/j.chemosphere.2019.01.176

Kreider M.L., Panko J.M., McAtee B.L., Sweet L.I., Finley B.L. (2010). Physical and chemical characterization of tire-related particles: Comparison of particles generated using different methodologies. *Science of the Total Environment*, 408(3): 652-659. doi: 10.1016/j.scitotenv.2009.10.016. Epub 2009 Nov 6.

Kwak J., Hongsuk K., Janghee L., Seokhwan L. (2013). Characterization of non-exhaust coarse and fine particles from on-road driving and laboratory measurements. *The Science of the Total Environment* 458–460: 273–82. <https://doi.org/10.1016/j.scitotenv.2013.04.040>.

Kwak, J., Sunyoup L., Seokhwan L. (2014). On-road and laboratory investigations on non-exhaust ultrafine particles from the interaction between the tire and road pavement under braking conditions. *Atmospheric Environment*, 97: 195–205. <https://doi.org/10.1016/j.atmosenv.2014.08.014>.

Lenschow P., Abraham H.-J., Kutzner K., Lutz M., Preuß J.-D., Reichenbacher W. (2001). Some ideas about the sources of PM10. *Atmospheric Environment*, 35: 23-33.

Lindenmuth B.E. (2006). An overview of tire technology. Chapter 1 in *The Pneumatic Tire: 2-27*. Report DOT HS 810 561 699pp. U.S. Department of Transportation, NHTSA (Ed.).

Lowne R.W. (1970). The effect of road surface texture on tyre wear. *Wear* 15(1): 57-70. [https://doi.org/10.1016/0043-1648\(70\)90186-9](https://doi.org/10.1016/0043-1648(70)90186-9).

Lundberg J., Blomqvist G., Gustafsson M., Janhäll S. (2017). Texture influence on road dust load. In: *Proceedings of the 22nd International Transportation and Air Pollution (TAP) Conference*, pp. 14. Switzerland. <http://urn.kb.se/resolve?urn=urn:nbn:se:kth:diva-222116> (may 2020)

Ma B., Xu H.-G., Chen Y., Lin M.-Y. (2017). Evaluating the tire wear quantity and differences based on vehicle and road coupling method. *Advances in Mechanical Engineering*, 9(5): 1-13.

Manas D., Manas M., Stanek M., Pata V. (2009). Wear of tyre treads. *Journal of Achievements in materials and Manufacturing Engineering*, 37(2): 538-43.

Mathissen M., Scheer V., Vogt R., Benter T. (2011). Investigation on the potential generation of ultrafine particles from the tire-road interface. *Atmospheric Environment*, 45: 6172-6179. doi:10.1016/j.atmosenv.2011.08.032

Panko J., McAtee B.L., Kreider M., Gustafsson M., Blomqvist G., Gudmundsson A., Sweet L. Finley B. (2009). Physio-chemical analysis of airborne tire wear particles. 46th Congress of the European Societies of Toxicology, Eurotox, 13-16 September 2009, Dresden, Germany (EU).

PIARC. (1995). International experiment to compare and harmonize skid resistance and texture measurements. Report reference 01.04.TEN 430pp. ISBN: 84-87825-96-6 <https://www.piarc.org/en/order-library/3826-en-International%20Experiment%20to%20Compare%20and%20Harmonize%20Skid%20Resistanc%20and%20Texture%20Measurements.htm>. (July 2020)

Pirjola L., Johansson C., Kupiainen K., Stojiljkovic A., Karlsson H., Hussein T. (2010). Road dust emissions from paved roads measured using different mobile systems. *Journal of the Air and Waste Management Association* 60(12): 1422–1433. <https://doi.org/10.3155/1047-3289.60.12.1422>.

Querol X., Alastuey A., Rodriguez S., Plana F., Ruiz C.R., Cots N., Massagué G., Puig O. (2001). PM10 and PM2.5 source apportionment in the Barcelona Metropolitan area, Catalonia, Spain, *Atmospheric Environment*, 35: 6407-6419.

Querol X., Alastuey A., Ruiz C.R., Artiñano B., Hansson H.C., Harrison R.M., Buringh E., ten Brink H.M., Lutz M., Bruckmann P., Straehl P., Schneider J. (2004). Speciation and origin of PM10 and PM2.5 in selected European cities. *Atmospheric Environment*, 38: 6547–6555.

Rajaratnam E., Walker D. (2019). Investigation of wheelhouse flow interaction and the influence of lateral wheel displacement. *Energies*, 12(17): 1-29. doi:10.3390/en12173340

Thivolle-Cazat E., Gilliéron P. (2006). Flow analysis around a rotating wheel. 13th Int. Symp. on Applications of laser techniques to fluid mechanics. 26-29 June, Portugal (EU).

Thorpe A.J., Harrison R.M., Boulter P.G., McCrae I.S. (2007). Estimation of particle resuspension source strength on a major London Road. *Atmospheric Environment*, 41: 8007-8020.

Thorpe A., Harrison R.M. (2008). Sources and properties of non-exhaust particulate matter from road traffic: A review. *Science of the Total Environment*, 400: 270-282.

- 934 Wik A., Dave G. (2009). Occurrence and effects of tire wear particles in the environment – A critical
935 review and an initial risk assessment. *Environmental Pollution*, 157(1): 1-11.
- 936 Wong J.Y. (2001): *Theory of ground vehicles*. John Wiley & Sons, INC. 3rd Ed., 528pp. ISBN 0-471-
937 35461-9.

938 Table captions

939 Table 1: Characteristics of the various types of pavements used in the test track experiments.

940

941 Figure captions

942 Figure 1: Illustrations (upper and lower panels) and schematic view (middle panel) of the
943 instrumental set-up implemented to monitor particulate emissions from the tire-road interface.
944 The orientation and velocity of streamlines were calculated at stabilized driving speeds using
945 Computational Fluid Dynamics (CFD) modeling with the Ansys Fluent application. The red
946 coloring represents the highest velocities.

947

948 Figure 2: Evolution of RoWP and TRWP emissions, in number (upper panels) and mass
949 (lower panels), measured on the road vs. driving speed. The empty and filled circles stand for
950 emissions per unit of distance and time, respectively. The square symbols refer to situations
951 where TRWP contamination by exhaust and brake particles was limited. While the fitting
952 curves account for the entire dataset, the square symbol data were used to formulate Equations
953 4a and b.

954

955 Figure 3: Changes in two key vehicle variables (driving speed and torque on the instrumented
956 wheel) and particulate emissions per kilometer as a function of the area traversed.

957

958 Figure 4: Photomicrographs and qualitative elemental compositions of brake wear particles
959 (BWP), RoWP and various surface areas of tires used on the road and in test track
960 experiments. BWP were collected on filters or impaction plates during braking. The sample
961 intake was set in the backspace of the wheel (mobile measurements) or lateral to the wheel
962 (measurements carried out using a chassis dynamometer). The proposed qualitative
963 compositions provide an overview of several dozen observations.

964

965 Figure 5: Standardized size distributions and relative contributions (in the form of bar charts
966 +1 S.E.) of RoWP and TRWP for various types of roads (upper panels) and driving situations
967 (lower panels). The proposed size distributions involve ELPI and OPC data. The data

968 associated with the 1.0-5.0 μm size range common to both devices were used to splice their
969 signals. The asterisk in the bar charts indicates that these were in fact relative contributions,
970 derived by dividing the emissions per time (dashed bars) or distance (solid bars) by the
971 corresponding average values obtained over the 25-km route.

972

973 Figure 6: Upper panel, relative contributions (+1 S.E.) of ultrafine, accumulation and coarse
974 RoWP modes for various types of pavements of specified macro- and microtextures. They
975 have been obtained by dividing the corresponding number concentrations by those of the
976 conventional AC2 pavement. Lower panels, contributions of ultrafine, accumulation and
977 coarse modes to total RoWP and TRWP concentrations (in number and mass) for one SMA
978 and two AC (aged 11 and 37 years) pavements.

979

980 Figure 7: Standardized TRWP concentrations plotted as a function of speed variation (panel
981 A: acceleration / panels B and C: deceleration) or kinetic energy recorded at the start of
982 braking (panel D) (error bars: ± 1 S.E.). A distinction was drawn between mild and heavy
983 decelerations as well as between data from different analytical instruments. Standardization
984 was performed by dividing with the values obtained during the lowest accelerations or
985 decelerations.

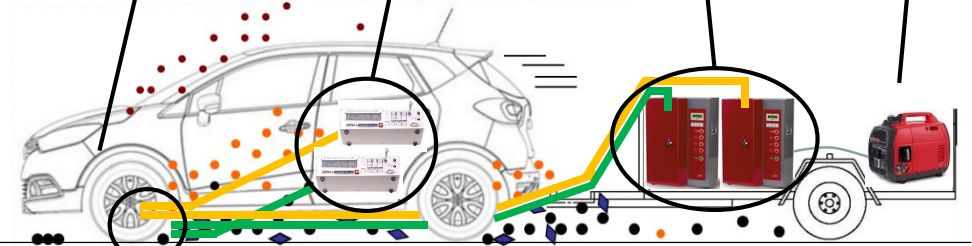


Instrumented vehicle

2 OPCs

2 ELPI devices

Inverter generator



Rear of the wheel

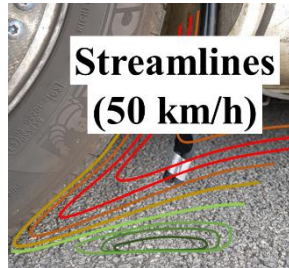
Backspace of the wheel



Air inlet

15 cm

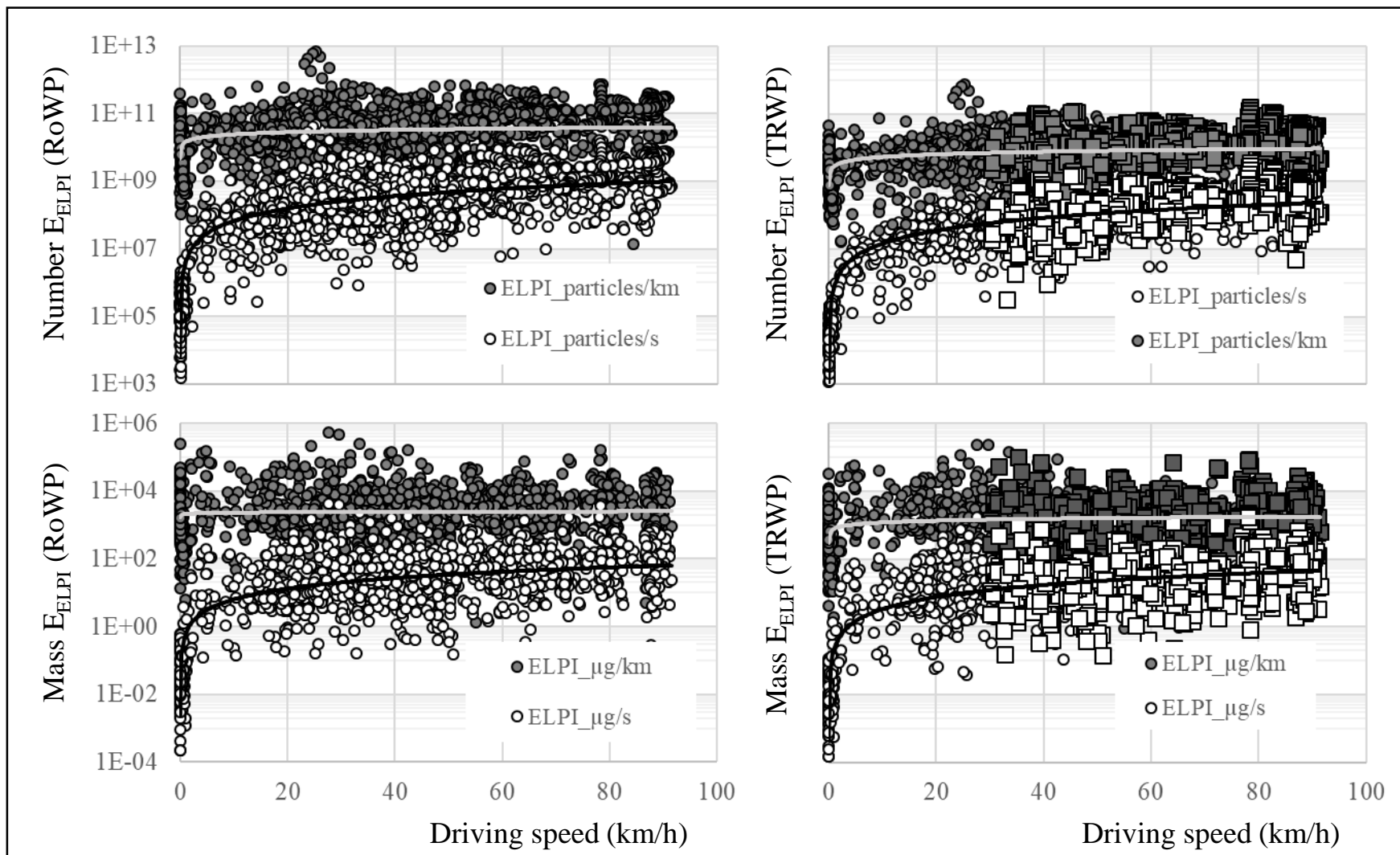
7 cm

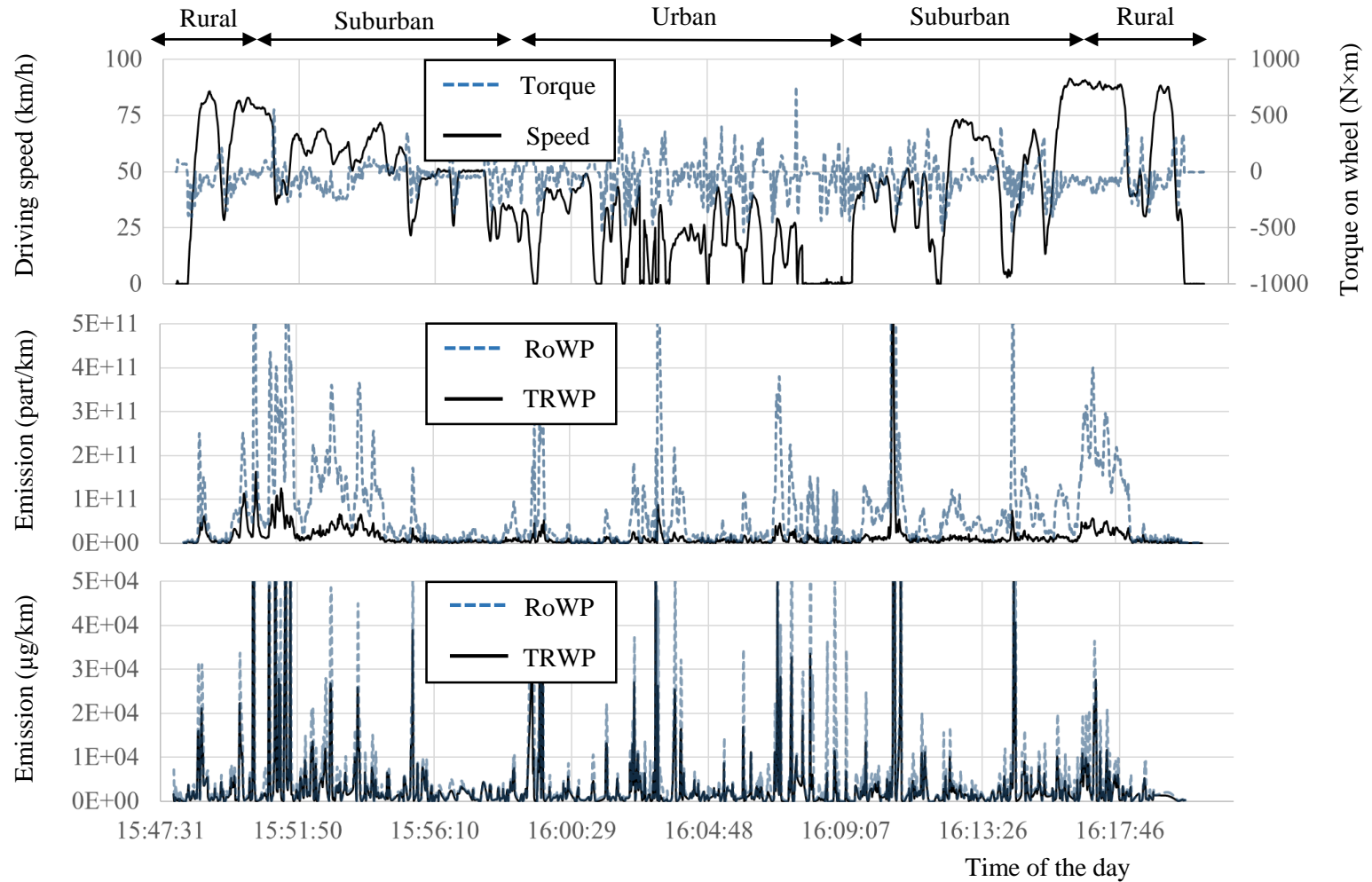


Streamlines
(50 km/h)



Air inlet

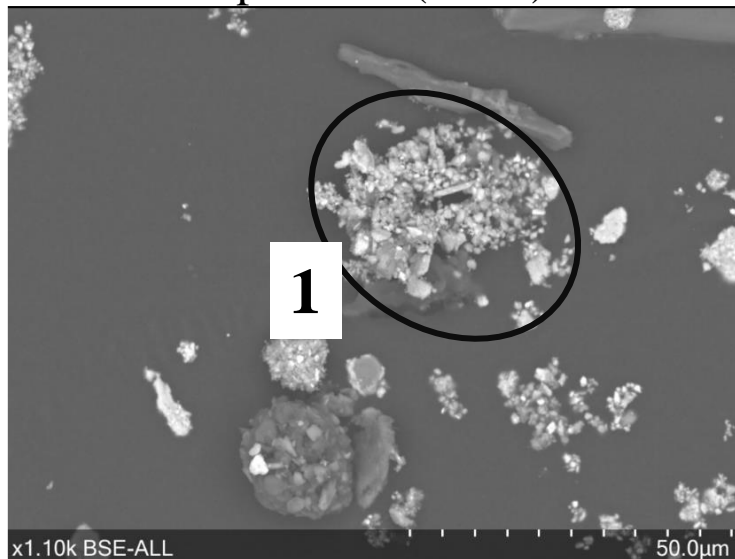




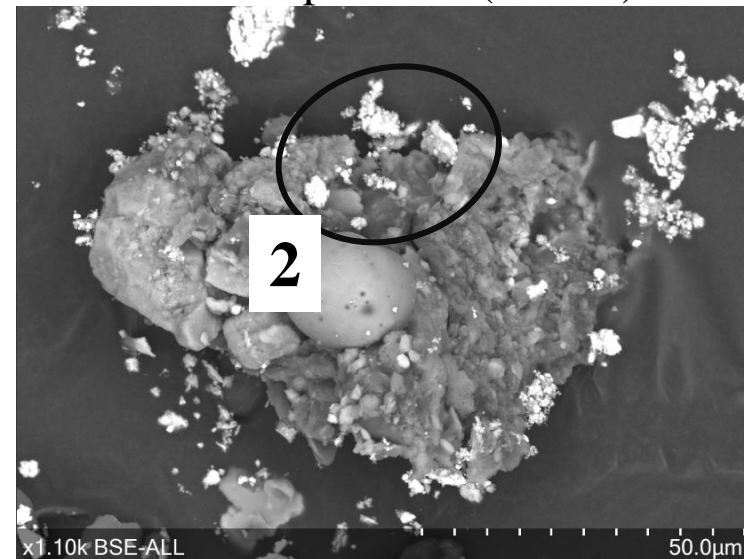
Qualitative compositions

BWP	1	2	3	4	5	6	
C	++	+	+	++	++	++	++
Fe	++	++	++	++	-	-	-
Si	-	-	++	+	+	-	+
Ba	+	+	-	-	-	-	-
Al	+	-	++	+	-	-	-
Zn	+	-	-	-	+	-	-

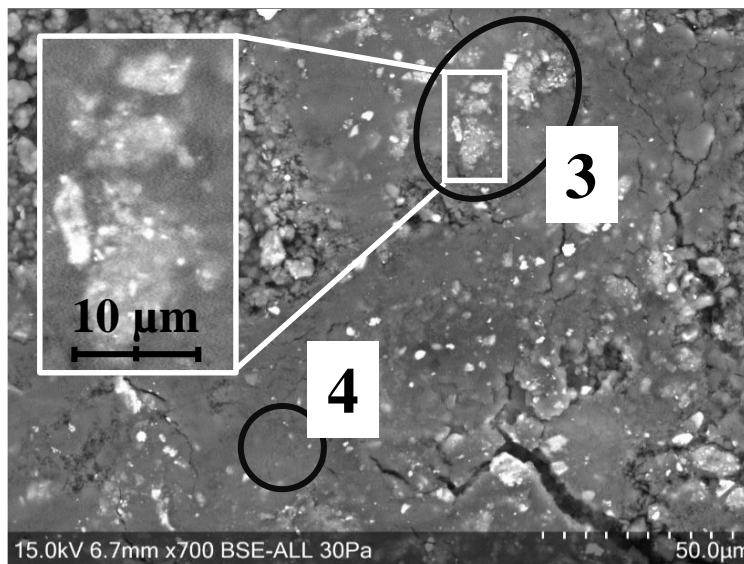
Break wear particles (BWP)



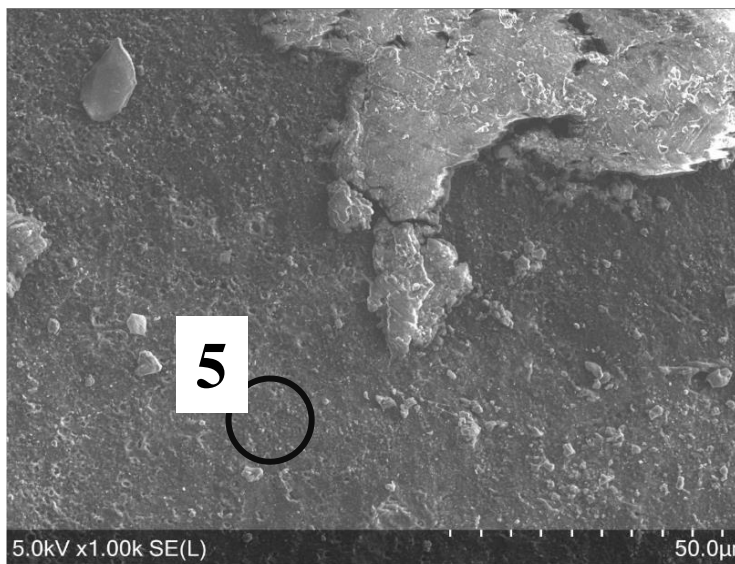
Rear of wheel particles (RoWP)



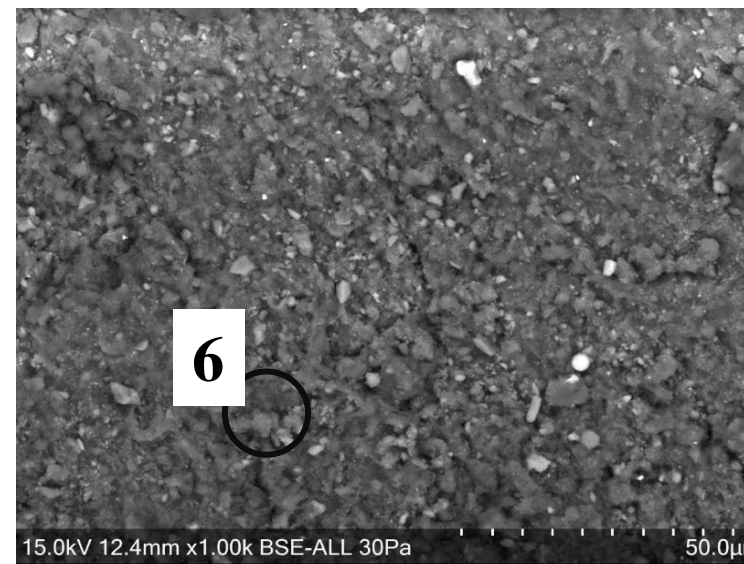
Tire tread



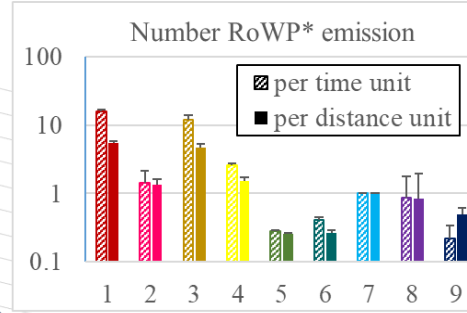
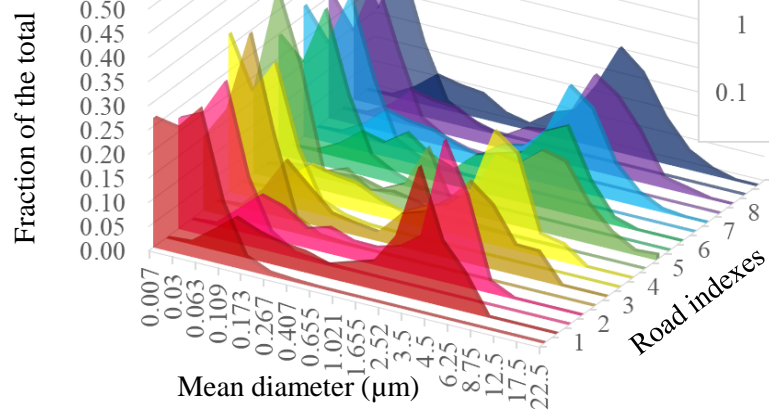
Tire groove



Tire sidewall

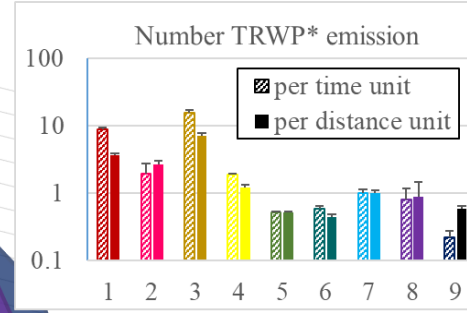
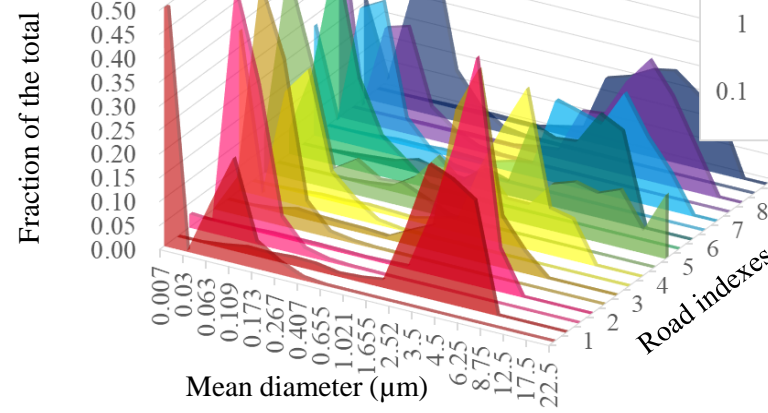


RoWP emissions for different roads



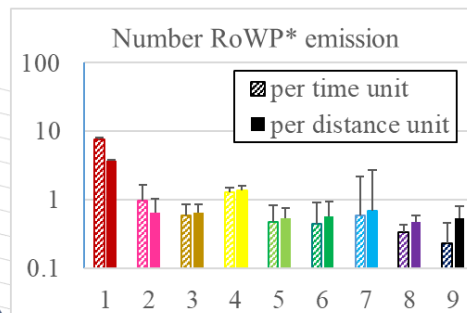
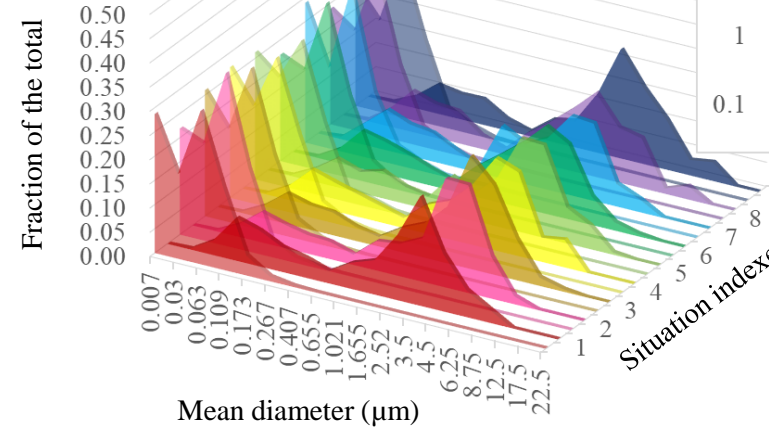
1. Motorways (88.5km/h)
2. Country roads (83.8km/h)
3. Cont. motorways (79.0km/h)
4. Ring roads (62.8km/h)
5. Overall test track (52.4km/h)
6. Remote suburban (50.1km/h)
7. Overall travel (41.9km/h)
8. Central suburban (38.3km/h)
9. City streets (17.6km/h)

TRWP emissions for different roads



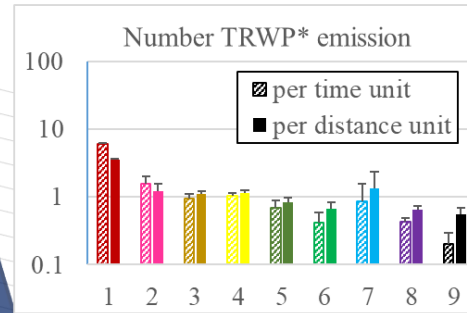
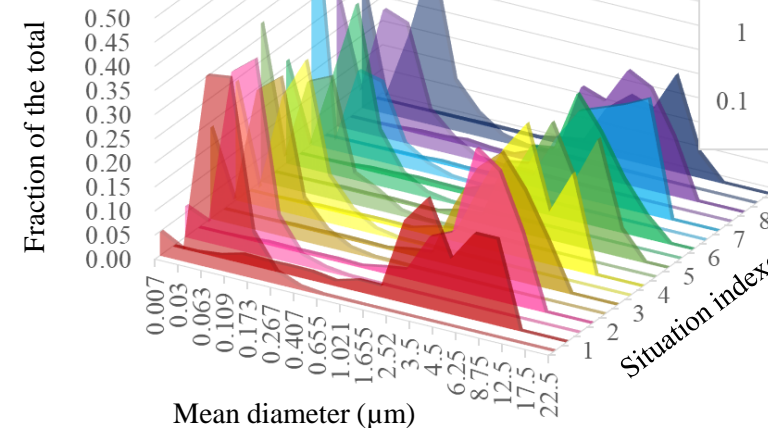
1. Motorways (88.5km/h)
2. Country roads (83.8km/h)
3. Cont. motorways (79.0km/h)
4. Ring roads (62.8km/h)
5. Overall test track (52.4km/h)
6. Remote suburban (50.1km/h)
7. Overall travel (41.9km/h)
8. Central suburban (38.3km/h)
9. City streets (17.6km/h)

RoWP emissions for different driving situations

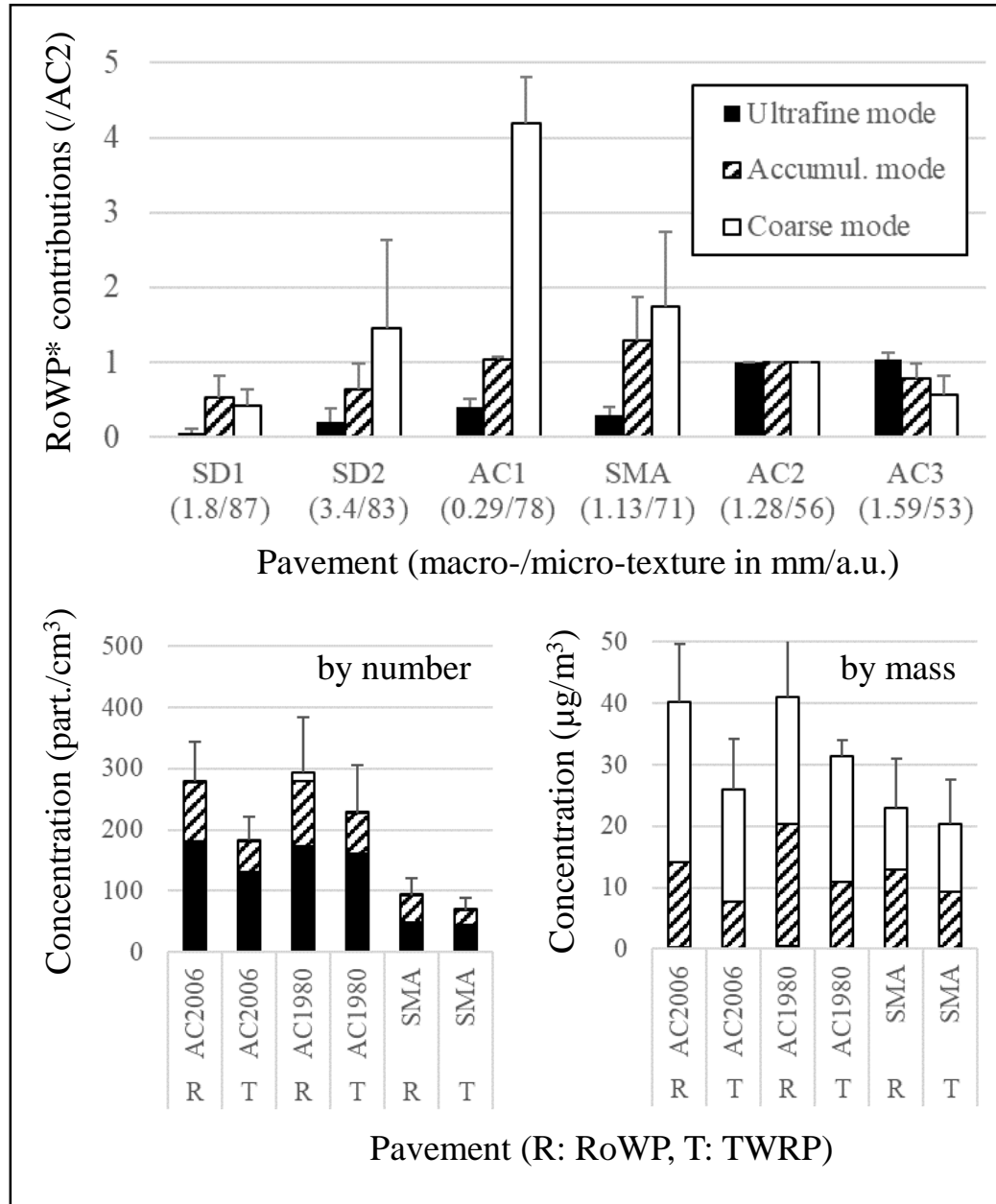


1. Tall bridges (59.4km/h)
2. Major junctions (47.4km/h)
3. Wide corners (35.8km/h)
4. Large roundabouts (35.5km/h)
5. Heavy decel. (31.2km/h)
6. Heavy accel. (29.6km/h)
7. Tight corners (24.3km/h)
8. Small roundabouts (24km/h)
9. Traffic lights (16.5km/h)

TRWP emissions for different driving situations



1. Tall bridges (59.4km/h)
2. Major junctions (47.4km/h)
3. Wide corners (35.8km/h)
4. Large roundabouts (35.5km/h)
5. Heavy decel. (31.2km/h)
6. Heavy accel. (29.6km/h)
7. Tight corners (24.3km/h)
8. Small roundabouts (24km/h)
9. Traffic lights (16.5km/h)



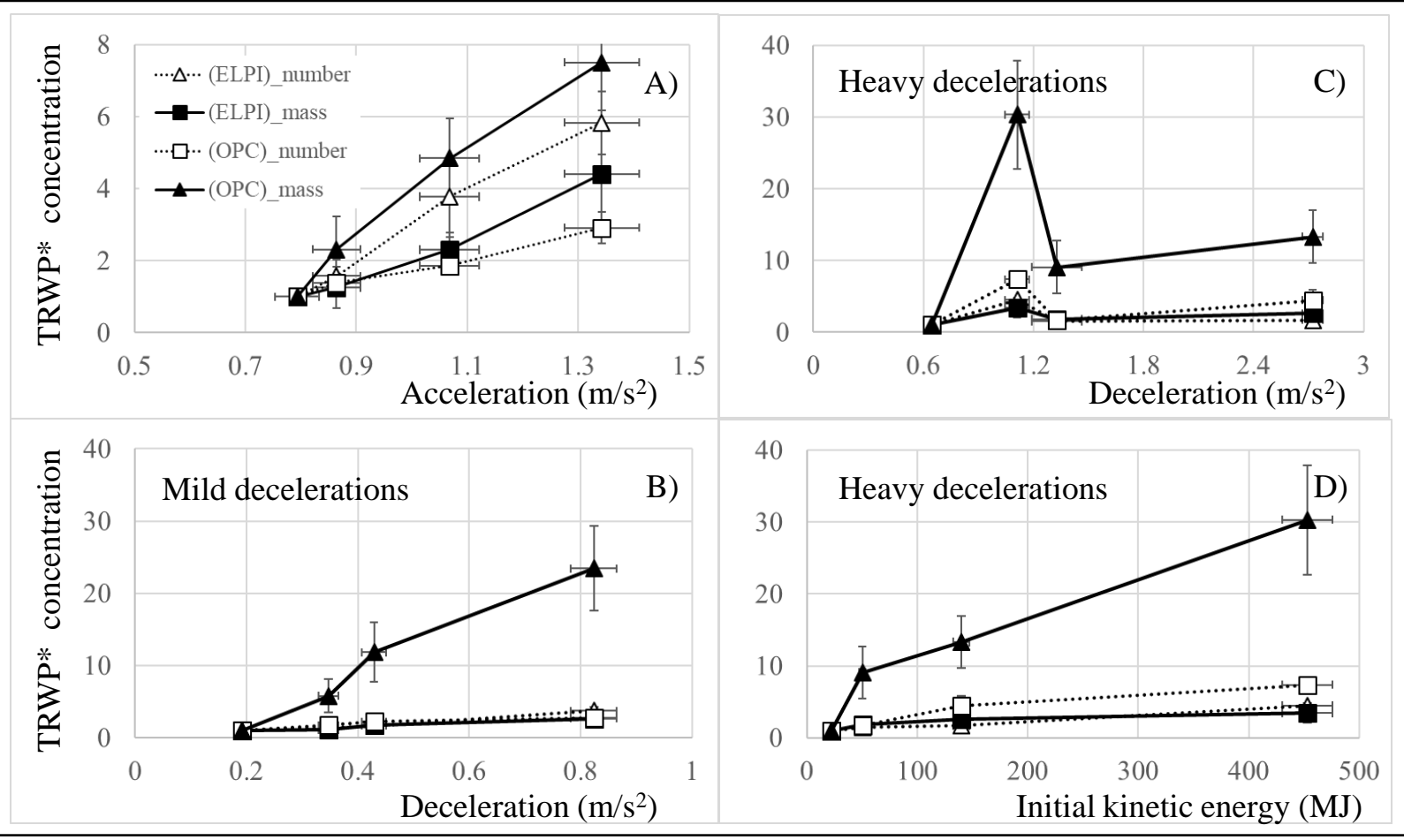





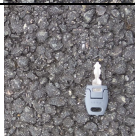




Table 1

Pavement name	Aspect	Description	Length (m)	Macro-texture (mm)	Micro-texture (a.u.)
AC1		High microtexture asphalt concrete 0/10	246	0.29	78
AC2		Conventional asphalt concrete 0/10	244	1.28	56
AC3		Porous asphalt concrete 0/6	221	1.59	53
AC ₂₀₀₆		Semi-coarse asphalt concrete 0/10	253	0.82	49
AC ₁₉₈₀		Aged semi-coarse asphalt concrete 0/10	100	1.25	56
SMA		Stone mastic asphalt 0/10	150	1.13	71
SD1		Low macrotexture surface dressing	144	1.8	87
SD2		High macrotexture surface dressing	100	3.4	83

Travel conditions

Road types

Rural Streets Motorway

Structures & equipment

Bridges Rotaries Lights

Passed areas

Urban
Suburban
Rural

The particles of interest

- Road dust (▢)
- Brake wear particles (●)
- Tire wear particles (●)
- Road wear particles (●)
- Rear of wheel particles (●, ●, ●, ▢)

Pavement texture, age, contamination...

Test track Tire track Tire tread

